INVESTIGATION OF THE FEASIBILITY OF AN OPTICAL IMAGING SYSTEM FOR THE APPLICATION OF IN VIVO FLOW CYTOMETRY

by

Phillip Martin

A Thesis Submitted to the Faculty of the

COLLEGE OF OPTICAL SCIENCES

In Partial Fulfillment of the Requirements

For the Degree of

MASTER OF SCIENCE

In the Graduate College

THE UNIVERSITY OF ARIZONA

2016

STATEMENT BY AUTHOR

The thesis titled *Investigation of the Feasibility of an Optical Imaging System for the Application of In Vivo Flow Cytometry* prepared by *Phillip Martin* has been submitted in partial fulfillment of requirements for a master's degree at the University of Arizona and is deposited in the University Library to be made available to borrowers under rules of the Library.

SIGNED: *Phillip Martin*

APPROVAL BY THESIS DIRECTOR

This thesis has been approved on the date shown below:

Arthur Gmitro
Professor of College of Optical Sciences

7-21-2016
Date

Acknowledgements

I would like to thank Professor Arthur Gmitro for providing me with an incredible opportunity for working in his lab. I thoroughly enjoyed the time spent together, regarding the experiments and discussions in the lab. My success is a result of his exceptional mentoring, guidance, and support. I would like to thank Professor Andrew Rouse for being incredibly supportive throughout the process of my Thesis work. He has always been available for aiding in helping me out with equipment, operation of equipment, experiments, and talking about devices employed in our experiments. I would like to thank Professor Khanh Kieu for electing to be on my committee. I would like to thank On target laboratories for providing the OTL38 contrast agent that was used for our fluorescent imaging. Also, I would like to thank Dr. Ghassan Mouneimne's lab in the University of Arizona Cancer Center for providing us with the PDX cancer cells we used for imaging. I would like to thank the CGRI lab group for aiding in the 3D printing of parts for our potential experiments. I would also like to thank the following lab group members: Tzu-Yu Wu and Hui Min Leung for providing me with technical feedback on the optical systems that were used for my experiments and for helping me with SolidWorks. I would like to give out a big thank you to my parents for their continuous guidance, love, and support. Without them, my time as a successful academic would not be possible. Finally, I would like to thank my closest friend and colleague at the College of Optical Sciences, Raj Patil, for his moral support and occasional insightful discussions.

Dedication

Dedicated to my Parents…..

Table of Contents

Contents

List of Figures

List of Tables

ABSTRACT

This thesis investigates the feasibility of employing an optical imaging system for the application of in vivo flow cytometry for detecting rare circulating tumor cells (CTCs) in vasculature. This investigation presented used three optical imaging configurations: a Nikon Eclipse E600 fluorescence microscope with a PIXIS 2048B CCD camera; a Nikon Eclipse E600 fluorescence microscope with a ThorLabs DCC 3240N CMOS camera; and a custom built confocal microendoscope with a ThorLabs DCC 3240N CMOS camera. These systems were employed to gain insight as to what signal to noise ratios and sensitivities are required to sufficiently detect fluorescently labeled cancer cells. This work presents general concepts of fluorescence and confocal microscopy, the experimental setups employed, and experimental measurements and results obtained. The experimental measurements involved the following: the simulation of flow cytometry by imaging green fluorescent microspheres, with a fluorescence excitation range of 505-515 nm and a diameter of 15μm, in a square crit tube moving on a translational stage, and imaging a selection of cells that included MCF10A breast cells (non-cancerous), OVCAR3 ovarian cancer cells, and patient derived xenogram (PDX) breast cancer cells, which express folate-receptor proteins on their surface. We fluorescently labeled these cells with the introduction of a new folate-receptor targeted fluorescent contrast agent OTL38, made by On Target Laboratories. The results established that we were able to image and detect fluorescence microspheres with a minimum signal to noise ratio (SNR) of 2.3 using the ThorLabs DCC 3240N camera on the Nikon Fluorescence microscope. We were able to image and detect the cells used on all three system configurations. Analyzing the different cell uptake efficacies of the contrast agent OTL38, we established that the SNR levels were variable when imaging PDX breast cancer cells. We propose future work to investigate possible effects on the variability of SNR results, as well as, and future steps in designing a real-time optical fluorescence imaging system for in vivo flow cytometry.

Chapter 1 Introduction

Motivation

In vivo flow cytometry is a potential approach for monitoring and analyzing the characteristics of various cancers, as well as the evolution of other diseases that can be analyzed through the vascular system. The spread of cancer is a phenomenon that is still not fully understood. One aspect that is not fully understood is the ability of cancer to spread to other host sites in the body and metastasize[1]. It is believed that metastasis may be due to individual cancer cells traveling through the vascular system, after having separated from a source tumor, and attaching to another host tissue. Hence, there is a need for an imaging system that could potentially detect these cells travelling through the vascular system.

1.2 Flow Cytometry

Flow cytometry is the measurement of cells through a flow system [2]. As cells flow through the system, they pass through a point of measurement. Typically this involves focusing light onto a target point of measurement. Fluorescence and scattered light from the specimen is then recorded by a detection mechanism. Some biological samples are inherently fluorescent, but it is more common to achieve fluorescence through the labeling of cells. Labeling of cells can be achieved by the use of fluorescent chemicals and antibodies. The value of this process is that it enables one to distinguish between different cell types in a heterogeneous population, as well as quantify the number of different subsets of cells.

1.3 OTL38

OTL38 is a new compound consisting of a folate receptor targeting molecule. The molecule is linked to a near-infrared (NIR) dye [3]. This enables the folate receptor targeting molecule to bind to cells that express a folate-alpha receptor. OTL38 is presently being investigated as an administered agent that can assist in surgical procedures, such as tumor removal. Tumors that consist of highly expressed folate-alpha receptor sites, such as ovarian cancers, serve as potential receptors for using this agent.

1.4 Experimental Setups of Different Systems for in vivo Flow Cytometry

Several approaches have been investigated to perform in vivo flow cytometry [4-7]. These techniques include what will be referred to as confocal in vivo flow cytometry, flow cytometry with two-photon microscopy, photoacoustic flow cytometry, and spectrally encoded confocal microscopy.

1.4.1 Confocal in vivo Flow Cytometry

The confocal in vivo flow cytometer typically employs a confocal fluorescence setup and is a non-imaging setup that acquires temporal signal. This involves a laser source illumination that is shaped into a line of light by a cylindrical lens and focused onto a small region in the sample. Emitted fluorescence is then reflected by a dichroic mirror onto an emission filter. The light is focused onto a confocal slit, which rejects out of focus light and onto a photomultiplier tube placed just behind the confocal slit. A data acquisition card at a sampling rate stores the data which can be displayed on a computer. Operating in parallel is a transillumination imaging system

for selecting an artery. Contrast was achieved by fluorescently labeling red blood cells (RBCs) with a DiD contrast agent and passing them through a 635nm laser illumination. As each cell passes through the laser, a burst of fluorescence is produced and temporal signal was accumulated. The study described in Ref. [4], by Y.Ding, J.Wang et. al., addresses the limitations of depth of signal measurement, due to the strong scattering of light in tissue. The enhancement of depth was achieved by using an innovative optical clearing agent, referred as an ear skin optical clearing agent (ESOCA), in lieu of glycerol. This agent was placed on a rat ear, where measurements were acquired, that minimizes scattering affects and improves the depth signal capabilities, as well as the signal to noise ratio (SNR).

1.4.2 Two-Photon Fluorescence Flow Cytometry

Two photon excitation fluorescence is a nonlinear optical technique that involves the absorption of two photons of approximately half the energy of a single photon fluorescence excitation. The molecule, once stimulated, emits fluorescence light just as it would in single photon fluorescence. To generate significant two photon fluorescence, the optical flux density of the excitation light must be very high. To achieve this, pulsed laser sources are employed that are focused into the sample. The emitted fluorescence is stronger where the beam is focused as opposed to where it is diffuse. Therefore, most of the fluorescence is generated from a very small finite volume near the focal point of the excitation beam. As a result, one does not need a confocal aperture to eliminate out of focus light. The study described in Ref. [5], by W. He, H.Wang et. al., involved utilizing two-photon microscopy for quantifying rare CTCs in vivo as a potential methodology for the diagnosis and evolution of cancer, as well as the assessment of response to therapy, and the

monitoring of residual disease following surgery. Contrast was achieved with different fluorescent contrast agents. Multiple contrast agents such as, DiD, folate-AlexaFluor 488, anti-FR polyclonal antibodies, and folate-FITC, were tested to analyze the different efficiency rates of cellular uptakes of each agent. In vivo results involved introducing (10^6) L1210A leukemia cells into mice, while injecting 5 nmol of folate-rhodamine per mouse. Intravital two-photon microscopy was used to detect the L1210A cells in the vasculature of the ear. Quantitative analysis of CTCs was conducted in larger, faster-flowing vessels, and temporal signals were acquired with one dimensional scanning along a direction perpendicular to a vessel. The study of CTCs originating before metastasis from a solid tumor was quantified in vivo. A metastatic tumor model was established with subcutaneous implantation of M109 murine lung cancer cells with moderate FR expression on the dorsal flanks of mice. 1.4 CTCs per min could be detected in vasculature after a two week period. By three and four weeks, 7 and 18 CTCs per min could be detected. In vitro results involved whole blood samples of 12 ovarian cancer patients with different pathologies: stages I-IV. All of these samples were administered 100 nM of folate-AlexaFluor 488. Except for the stage I and stage II patients, all of the patients exhibited CTC counts significantly greater than background (<6CTCs/ml). It was established that human CTCs could be selectively labeled and quantitated at a concentration of approximately 2CTCs per ml.

1.4.3 Photoacoustic Flow Cytometry

Photoacoustic flow cytometry involves nonradiative conversion of absorbed light energy into heat (photothermal effect) that is accompanied by acoustic waves (photoacoustic effect). This

involves absorption of laser radiation by a single cell that induces a temperature increase in endogenous and exogenous structures (nanoparticles). Emitted acoustic waves are detected by an ultrasonic transducer to acquire temporal signal acquisition of each cell. The acoustic resolution is dependent on the beam width. The signal of each cell is dependent on the exposure to the incident beam and the absorption of optical energy. The laser pulse rate is set to the ratio of the flow velocity divided by the beam width to acquire signals of the cells moving through the vessel. In the study presented in Ref. [6], by E. I. Galanzha and V.P. Zharov, both labeled and label-free detection methods were presented in this study. Label-free methods involved the study of circulating melanoma cells. The high PA signals of pigmentation of melanin serves as contrast to that of the background signals of RBCs in the NIR range. Labeled techniques involve using nanoparticles that bind preferentially to CTCs. In vivo data demonstrated that this technique can achieve a sensitivity of CTCs of 1CTC per 40ml of blood volume with a throughput up to 10mL per minute.

1.4.4 Spectrally Encoded Flow Cytometry

Spectrally-encoded flow cytometry (SEFC) is a reflective confocal microscopic technique that employs an endoscopic probe in which illumination light from an optical fiber is diffracted by a transmission grating. Each wavelength in the illumination spectrum is diffracted at a unique angle and focused on a distinct transverse location on the sample by a high-NA objective lens. Light reflected from the sample is collected back through the fiber and re-dispersed onto a 1D detector to form a line image. The fiber core aperture serves to reject out-of-focus light, and therefore, it

serves as both the illumination source and detection pinholes of the confocal system. Scanning in the orthogonal direction is achieved passively by the flow of cells through the line of measurement. A two dimensional image of a cell is achieved in which one axis is encoded by wavelength and the other (the direction of flow) is encoded by time. The relatively small field of view of the confocal spectrally encoded line limits the ability to identify capillary vessels below the tissue surface for confocal imaging. In the work described in Ref. [7], by L. Golan, D. Yeheskely et. al., an additional widefield imaging channel was added, which increased the field of view sufficiently to identify vessels. A beam from a green light-emitting diode was collimated and coupled into this second imaging channel using a dichroic mirror. The light backscattered from the tissue was imaged using a CCD camera. Due to the absorption properties of hemoglobin in the green spectrum, blood vessels were viewed as dark regions on a bright background. A pair of crossed polarizers was used to further enhance image contrast. The in vivo reflectance confocal microscope system was used to continuously visualize the flow of blood cells in a flow chamber and in the oral mucosa.

1.5 Overview

Although the sections above show that some preliminary research work has been done in the area of in vivo flow cytometry, it is still not an established technique. The objective of this thesis is to investigate the feasibility of using 2D en face fluorescent optical imaging techniques, with the fluorescent contrast agent OTL38, as a way to detect rare CTCs in vasculature flow. The focus was to experimentally compare and contrast two optical systems, an in house scanning fluorescence confocal microendoscope and a Nikon Eclipse E600 fluorescence microscope, for

their ability to detect fluorescently labeled tumor cells. The folate receptor targeted contrast agent OTL38, from On-Target Laboratories, was used to label tumor cells. Chapter 2 will provide a brief overview of both normal fluorescence microscopy and fluorescence confocal microscopy and the experimental setups of the two optical systems. Chapter 3 discusses the comparison of the relative optical throughput of both systems and other performance metrics. Chapter 4 discusses the experiments conducted, as well as the measurements, quantitative analyses, and results obtained. The experiments include: imaging of fluorescent microspheres, PDX breast cancer cells, and OVCAR3 cancer cells. Chapter 5 discusses the results and conclusions of the work, as well as, future work to establish the feasibility of using a fluorescent targeting agent for detecting and imaging rare CTCs in vivo.

Chapter 2 Fluorescence and Confocal Microscopy

2.1 Introduction

This chapter discusses the basic principles concerning both wide-field fluorescent microscopy and confocal fluorescent microscopy. It also presents technical information concerning the two optical systems used for the experiments performed in this work. The optical systems presented are a Nikon Eclipse E600 wide-field fluorescent microscope and a custom built confocal microendoscope.

2.2 Conventional Fluorescence and Confocal Microscopy

2.2.1 Fluorescence Microscopy

In a conventional fluorescence microscope, the excitation light is typically obtained from a broadband light source, such as an arc lamp that is filtered to a narrow wavelength band by passing the light through an excitation filter that transmits the desired excitation spectrum. This excitation spectrum is then reflected by a dichroic mirror and focused by an objective lens onto a fluorescent specimen. A portion of the emitted fluorescent light is collected back through the objective lens, and is transmitted by the dichroic mirror while eliminating the back-reflected illumination wavelength. An emission filter is often introduced to limit the spectral range of the detection to a specific wavelength region of interest. A tube lens is used to focus the light onto an imaging detector, such as shown in Figure (2.3) [8], or the light can be sent through a tube lens and an eyepiece lens for direct viewing of the fluorescence image by the observer.

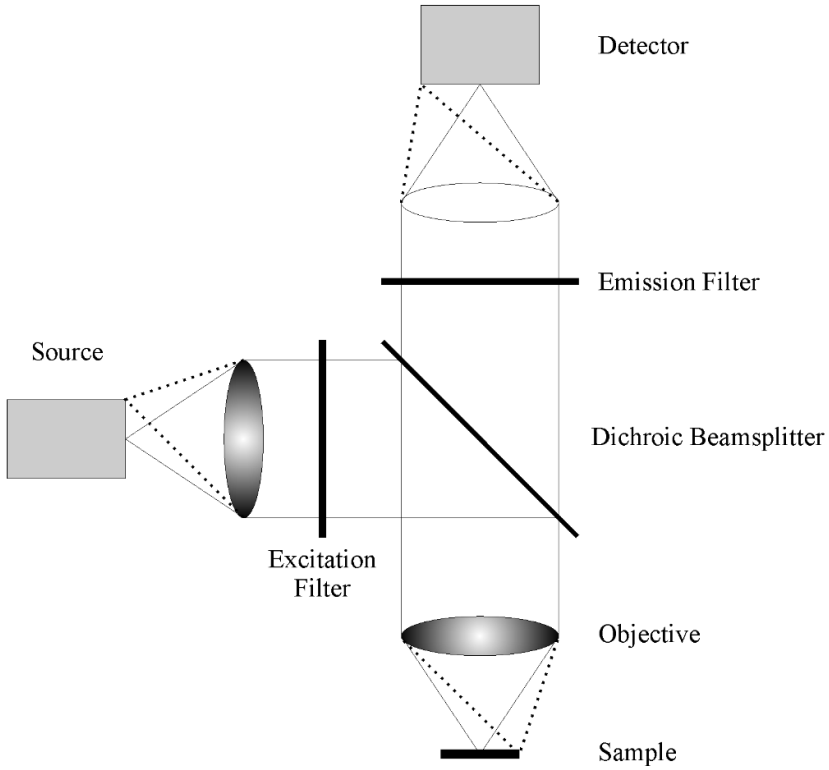

Figure 2.1. Conventional fluorescence microscope. Diagram courtesy of A. Rouse (2004)

If we want to relate the NA to overall resolution of the system, we need to invoke some diffraction concepts, which have been established [9-11].

2.2.2 Confocal Microscopy

Confocal microscopy involves use of a point source illumination that is imaged onto a small region, or point, in the sample. The fluorescent light emitted from the sample is transmitted back through a dichroic mirror and, typically, an emission filter, and re-imaged onto a confocal pinhole aperture. The combination of the focused point illumination and detection sensitivity of the pinhole image at the sample create a situation where the confocal microscope system is much more highly sensitive to the light coming from the confocal location of the point illumination and detection sensitivity. Scanning the sample in both lateral directions enables a two dimensional

image to be obtained at a specific depth in the sample. Figure (2.6) shows a schematic diagram of a conventional confocal scanning microscope [8]. The scan head typically consists of two galvanometer mirrors that scan the illumination and pinhole detection sensitivity function simultaneous across the sample.

The intensity PSF for a confocal microscope depends on both the illumination PSF; and the detection PSF. As an object moves through the beam (or the scan head moves the beam across the object), the amount of light reaching the detector at any location of the object is the product of the illumination irradiance and the detection sensitivity, for a point scanning system.

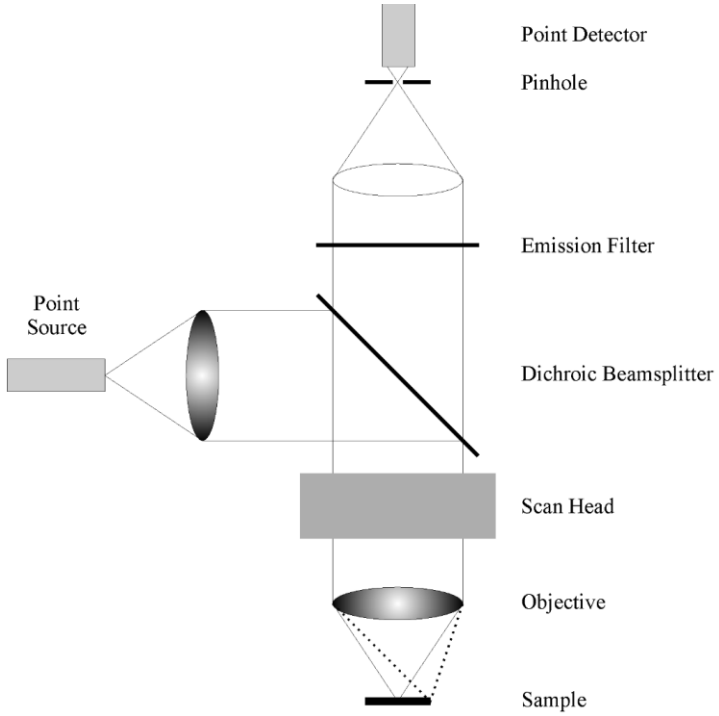

Figure 2.2. Conventional scanning confocal microscope. Diagram courtesy of A. Rouse (2004)

Essentially the resolution is improved by the point illumination and the addition of the pinhole aperture. Although there is the potential for improvement in lateral resolution in a confocal microscope, this improvement is almost never realized because of the finite size of the

pinhole employed to collect enough light. However, the optical sectioning property (that is the selective sensitivity to light from a given depth location) can still be retained even if the lateral resolution is not significantly improved with a finite size pinhole. The major unique property of the confocal microscope is that it has an axial (or depth) resolution, basically the thickness of the optical section.

2.3 Nikon Eclipse E600

The first imaging system used in our experiments was a Nikon Eclipse E600 widefield fluorescent microscope. The Nikon Eclipse E600 is a commercially designed and constructed unit. Used as a fluorescence microscope, the E600 does not feature scanning optics, nor does it yield optical sectioning capabilities. It does employ these features when a C1 confocal attachment is added. However, this attachment was not used for our experiments.

2.3.1 Illumination Optics

The illumination of the Nikon Eclipse E600 uses a halogen broadband light source for bright field imaging. A mercury xenon arc lamp is used for fluorescence imaging with a set of filter cubes for choosing the desired excitation/emission wavelength band. The filter cubes employed for our experiments included a G-2A, and an ICG filter cube. Table (2.1) shows the excitation, emission and dichroic cut-on spectra for each cube. The excitation wavelength band is selected by the excitation filter and is redirected by a dichroic beam splitter onto the sample through the objective lens. The objective is achromatic for brightfield imaging which corrects for chromatic aberrations. There are multiple objective lens configurations on this unit: a 2X/.06 objective; a 4X/0.13 objective; a 10X/0.3 objective; a 20X/0.75. A set of neutral density (ND) filters were

employed to reduce the excitation illumination irradiance. The ND filters employed were a ND4, ND8, and ND16 filter. The combination of the filters reduces the illumination irradiance by a factor of 512. The resulting irradiance is 1/512 of the illumination irradiance with no filters in place.

Cube	Excitation (nm)	Emission (nm)	Dichroic (nm)
G-2A	510-560	590	575
ICG	748-789	814-851	800

Table 2.1. This data shows the different filter cubes used for the Nikon Eclipse E600.

2.3.2 Detection Optics

Once the incident fluorescence excitation light reaches the sample the emitted fluorescence is collected back through the objective and is transmitted through the dichroic mirror and emission filter. A tube lens, with a focal length of 200mm, focuses the light onto an intermediate image plane. The light expands past the intermediate image plane and is re-focused by an imaging lens onto a PIXIS 2048B CCD camera system manufactured by Princeton Instruments. The second camera used on the Nikon system is a ThorLabs DCC 3240N CMOS camera. Both of these cameras can be used for fluorescence imaging. The PIXIS camera was used as a standard for imaging performance. It cannot be applied effectively for in vivo flow cytometry due to its slow frame rate frequency (1 frame per second). The PIXIS 2048B mount has a 1X imaging lens which images the intermediate imaging plane onto the detector. This does not have an effect on the system's numerical aperture in image space (intermediate image or detector plane image). Figure (2.3) shows a plot depicting the quantum efficiencies through the spectral range of the PIXIS 2048B, and table (2.2) shows general performance specifications [12]. The detector has 2048X2048 pixels with a pixel size of 13.5 µm x 13.5 µm. It has a quantum efficiency of 80-95% in the visible

spectrum, but falls to about 74% in the NIR region. The camera is peltier cooled, and can go down to a temperature of -55^{0}C. It is a 16-bit camera, which means that the digital readout range is scaled as, $0 \leq S_{Full} \leq 2^{16}$. The PIXIS 2048B has a full well capacity of 100,000e^-. It has a maximum gain setting of 4. This is an amplifier gain at the readout that converts a quarter of the full well charge to the maximum voltage that yields the maximum analog-to-digital output. The PIXIS 2048B interfaces with the software WinView in which all digital imaging operations can be setup and performed.

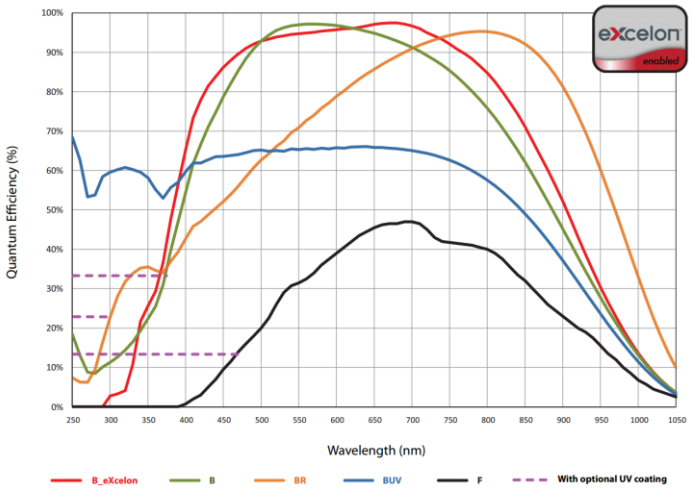

Figure 2.3. Plot of the quantum efficiency of PIXIS 2048B. The plot is labeled green. Retrieved from http://www.princetoninstruments.com/userfiles/files/assetLibrary/Datasheets/Princeton_Instruments_PIXIS_2048_eXcelon-N5_1-10_22_14.pdf

CCD UV coating	Optional UV coating
Quantum efficiency	See graph, next page
CCD format	2048 x 2048 imaging pixels; 13.5 x 13.5-µm pixels; 100% fill factor
Imaging area	27.6 x 27.6 mm (optically centered)
Lens mount	F-mount with integral 45 mm shutter
Deepest cooling temperature	< -70°C (typical), -60°C (guaranteed) with CoolCUBE II liquid circulator < -65°C (typical), -55°C (guaranteed) with air
Thermostating precision	±0.05°C
Cooling method	Thermoelectric air or liquid cooling (CoolCUBE II required)
Full well: Single pixel Output node	100 ke- (typical), 80 ke- (min) 1000 ke- (typical), 800 ke- (min)
ADC speed/bits	100kHz/16-bit and 2MHz/16-bit
System read noise @ 100 kHz @ 2 MHz	3.5 e- rms (typical), 5 e- rms (max) 12 e- rms (typical), 16 e- rms (max)
Vertical shift speed	32.2 µsec/row (programmable)
Non-linearity	<2% @ 100 kHz
Software selectable gains	1, 2, 4 e-/ADU (low noise input); 3.5, 7, 14 e-/ADU (high capacity output)
Operating systems supported	Windows 8/7 (64-bit) and Linux (64-bit), Windows 8/7/XP (32-bit)
Data interface	USB2.0 (5m interface cable provided); Optional Fiberoptic interface is available for remote operation
I/O signals	Two MCX connectors for programmable frame readout, shutter, trigger in
Operating environment	+5 to +30°C non-condensing
Certification	CE
Dimensions / Weight	19.51 cm (7.67") x 11.81 cm (4.65") x 11.38 cm (4.48") (L x W x H) / 2.5 kg (5.5 lbs)

Table 2.2. List of performance specifications for the PIXIS 2048B Retrieved from http://www.princetoninstruments.com/userfiles/files/assetLibrary/Datasheets/Princeton_Instruments_PIXIS_2048_eXcelon-N5_1-10_22_14.pdf

2.4 Confocal Microendoscope

The confocal microendoscope used in our experiments is a custom built optical scan unit (OSU) designed and built by Tzu-Yu Wu coupled to a flexible fiber-optics based probe [13]. Figure (2.4) shows a diagram of the OSU. It features three main components. These components include an illumination arm, scanning optics, and a detection arm. The OSU utilizes a multi-wavelength laser source, iFLEX Viper made by Qioptiq, with three wavelengths: 488 nm, 640 nm, and 780 nm. The OSU corrects for chromatic aberrations throughout a broad band wavelength range (486 nm – 850 nm) such that it can accommodate a wide range of excitation and emission wavelengths for fluorescent imaging using different fluorescent contrast agents. The camera system utilized for the OSU is a ThorLabs DCC 3240N CMOS camera.

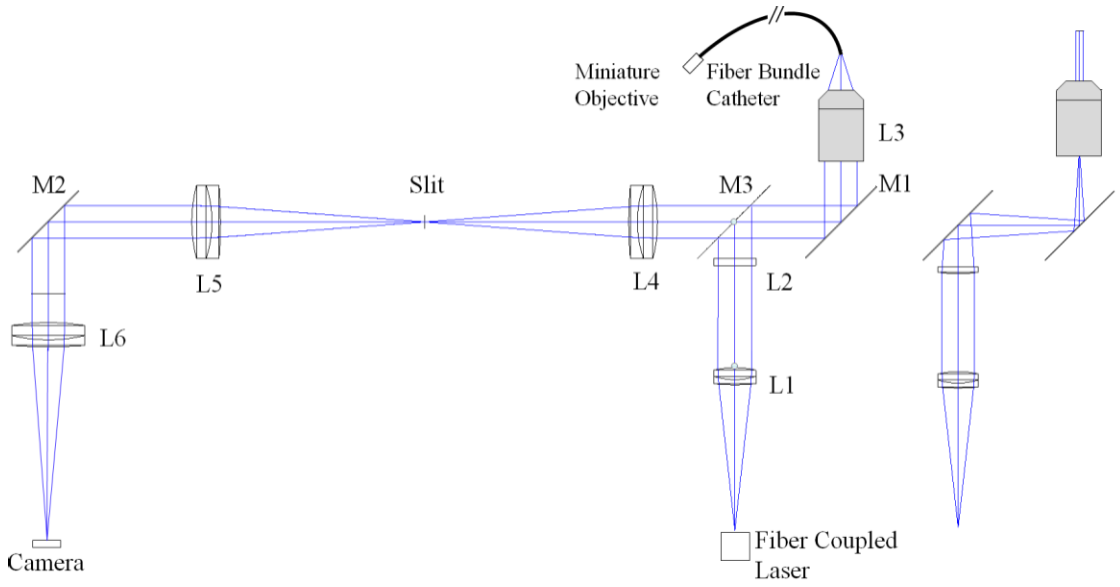

Figure 2.4. Diagram of OSU. Courtesy of T. Wu (2015)

2.4.1 Illumination Arm

The illumination arm involves light from the fiber coupled laser being expanded and collimated by an achromatic doublet that is diverted by a dichroic mirror (M3). The light is shaped into a transverse illumination line by the combination of a cylindrical lens (L2) and an Olympus 10X/0.3 objective (L3). The illumination line is scanned over the proximal end of the fiber by a scan mirror (M1). Light is transmitted to the distal end of the fiber and focused onto a specimen by a miniature objective lens.

2.4.2 Detection Arm

After the excitation wavelength is incident onto the sample, fluorescent light is collected back through the miniature objective lens and transmitted back through the fiber bundle to the proximal end of the fiber. The light is collected by the objective (L3), de-scanned by the scan mirror (M1) transmitted through the dichroic mirror (M3), and focused by an achromatic doublet (L4) onto the confocal slit. The confocal slit serves to reject out of focus light. The light is

expanded and collimated by another achromatic doublet (L5) and is scanned by a second scan mirror (M2). With an achromatic doublet (L6), light is focused onto a ThorLabs DCC 3240N CMOS. The DCC 3240N has a detector size of 1280 X 1024 pixels with a pixel size of 5.3 X 5.3 µm. It is typically set to a frame rate of 30 frames per second, but it can be operated to run at 60 frames per second. The scan mirrors are typically set to half the frequency of the frame rate, so each scanning direction coincides with one frame acquired by the camera. The DCC 3240N has a full well capacity of 8400 e^- with a maximum gain setting of 4, which maps a quarter of the full well capacity to the maximum digital output. The quantum efficiency of the DCC 3240N is ~70% in the visible spectra, but it falls to ~47% at 810 nm [14]. Figure (2.5) shows a plot for the quantum efficiencies for a spectral range of the DCC 3240N.

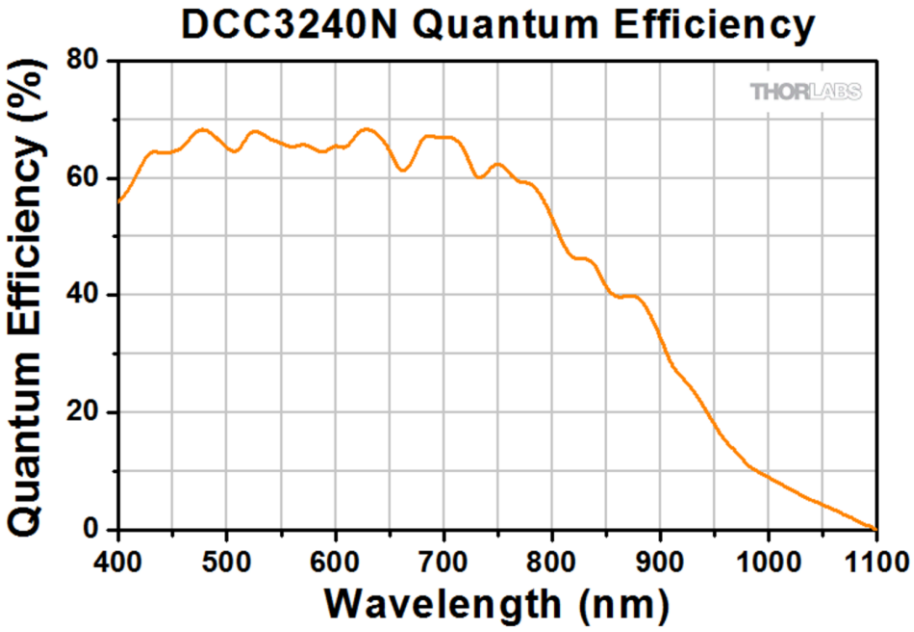

Figure 2.5. Plot of quantum efficiencies of DCC 3240N. Retrieved from https://www.thorlabs.com/newgrouppage9.cfm?objectgroup_id=4024&pn=DCC3240N

The DCC 3240N camera operates as a 10-bit camera. This means that the maximum digital readout scales to $S_{Full} = 2^{10}$. A labview program was used to set the camera to map 10-bit data

into 8-bit data. The 10-bit to 8-bit mapping conversion is shown in figure (2.6). The mapping of 10-bit to 8-bit data involves a non-linear gamma curve conversion with two knee cutoff points. It is essentially boosting dim gray-scale values at the expense of dynamic range in the bright gray-scale values. The mathematical expressions concerning the knee cutoff points are described in an E2V chip data sheet [15].

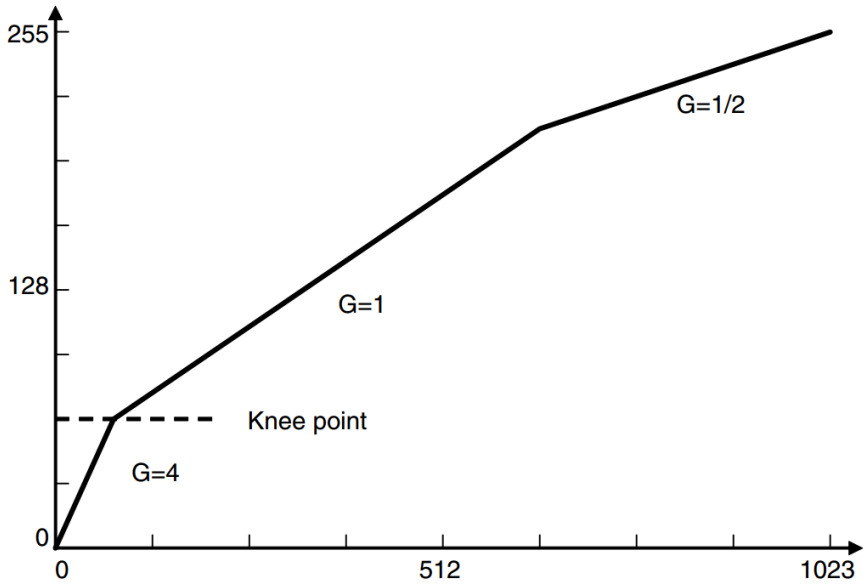

Figure 2.6. The mapping plot converting 10-bit data to 8-bit data. Retrieved from http://www.e2v.com/content/uploads/2014/02/DSC_EV76C661.pdf

Chapter 3 Comparison of Two Systems

3.1 Transmission and Sensitivity Comparison

This section presents a rough calculation of the relative transmission coefficient (T) of our confocal microendoscope system compared to the Nikon Eclipse E600. We wanted to establish the relative optical throughput of the confocal microendoscope relative to the Nikon system. This served as a way to analyze relative system performance in our experimental data. The confocal microendoscope has a lower optical transmission coefficient because of the fiber bundle employed in the system and the increased number of optical components. We used our results for transmission and known properties of the optical system to determine how many photoelectrons are being produced for each incident photon on the ThorLabs CMOS detector in the confocal system and on the PIXIS CCD detector in the Nikon system. We also calculated the relative SNRs of both systems. This analysis was achieved by measuring digital signals on both systems, measuring the excitation irradiance in object space, using radiometric analysis, and relationships concerning digital readouts as well as the known quantum efficiencies of our camera systems.

3.1.1 Procedure

The procedure for making these measurements involved taking a piece of tissue paper, placing it on a glass slide, and staining it with a 5:1 ratio (50µL/10µL) of phosphate buffered saline (PBS) to OTL38. For the Nikon system, we placed a glass coverslip over the sample for imaging because

the Nikon objectives are designed to operate with standard thickness glass coverslips. We measured the incident (excitation) radiation power with a power meter to be 5 mW, using the ICG cube in place and a 10X/0.3 objective lens. The camera used on the Nikon microscope was the PIXIS 2048B CCD camera system, set to an integration time of 30 msec and a gain of 4. Since the full well capacity of the PIXIS is 100,000e^-, the gain of four reduces the effective full well capacity for maximum digital signal to 25,000e^-. The quantum efficiency of the camera is approximately 74% at 810nm, which is the center emission wavelength of the ICG cube and the emitted OTL fluorescence. For the measurement with the confocal system, we took off the coverslip from the sample since the miniature objective lens on the end of the probe has a cover slip. The objective lens attached to the proximal end of the fiber is a 10X/0.3 lens. In the confocal system, the incident excitation power from the 780nm laser source was measured to be 1.3 mW on the object. The camera system used was a ThorLabs DCC3240N CMOS camera, which was set to an integration time of 30 msec and a gain of 4. The DCC3240N CMOS camera has a full well capacity of 8400e^-. Therefore, with a gain of 4 the effective full well capacity corresponding to the maximum digital value is reduced to 2100e^-.

3.1.2 Applied Radiometric Concepts

Regarding the radiometric concepts that were applied in this measurement, we consider a simple optical system, as shown in figure (3.1). Since one objective of this calculation was to compare the transmission of light through the confocal system relative to the Nikon, we adhere to the simple argument that for a uniform Lambertian source object the radiance in image space is equal to the radiance in object space times the transmission coefficient of the optical system, such that

$$L_{img} = L_{obj} * T, \quad (3.1)$$

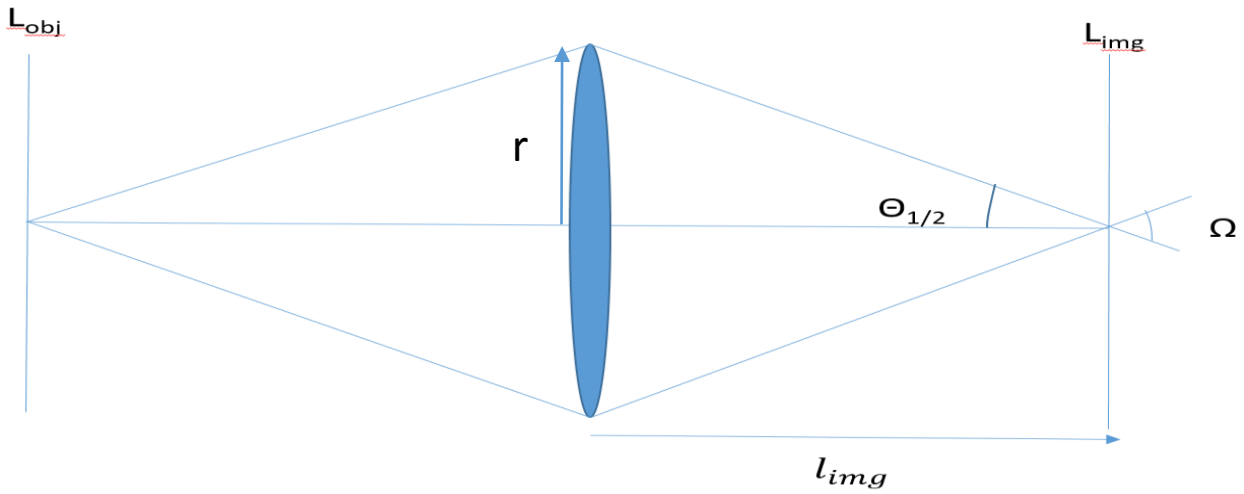

Figure 3.1. Simple optical system depicting the solid angle

where L_{obj} is the radiance in object space, L_{img} is the radiance in image space, and T is the transmission coefficient of light passing through the system. The irradiance in the image plane is given by

$$I_{img} = L_{img} * \Omega, \quad (3.2)$$

where I_{img} is the irradiance in image space, and Ω is the solid angle of the optical beam in image space. The solid angle is the ratio of a subtended spherical surface area of a beam divided by the square of the sphere radius from the source, which for the light in image space can be approximated as the pupil area of the optical imaging component (lens) divided by the square of the image distance from the lens to the image. Thus, the solid angle is given by,

$$\Omega = \frac{\pi * r^2}{l_{img}^2}. \quad (3.3)$$

The ratio of the pupil radius divided by the image distance yields the half-angle, which for small angles is given as:

$$\theta_{1/2} = \frac{r}{l_{img}}. \tag{3.4}$$

Plugging this relationship into equation 3.3 we obtain the solid-angle as,

$$\Omega = \pi * \Theta_{1/2}^2. \tag{3.5}$$

With small angles and index of refraction equal to air, the half-angle is approximately equal to the numerical aperture (NA) of the imaging system. Therefore, the expression for the solid angle assumes the form:

$$\Omega = \pi * NA^2. \tag{3.6}$$

Knowing the solid angle and the irradiance incident onto the image plane, one can calculate the amount of electromagnetic energy incident on a given pixel. The energy is given as

$$E = I_{img} * A_{pixel} * t_{ex}, \tag{3.7}$$

where A_{pixel} is the area of a pixel, and t_{ex} is the integration time or exposure time of the incident field.

3.1.3 Numerical Apertures of Both Systems

We determined the NAs of both systems in image space to calculate the solid angles for both systems. The solid angle is used in the final expression for the transmission calculation as will be established in a later section. To determine the effective NA of the Nikon Eclipse E600 in image space, we use the lateral magnification of the objective lens and tube lens imaging system, as is

depicted in figure (3.10). The 10X objective lens from Nikon has an NA_{obj} = 0.3 and a working distance of 16mm. When combined with the tube lens the imaging system has a lateral magnification of 10. The NA of the system in the intermediate image plane is therefore equal to the NA_{obj} divided by 10 which equals 0.03. Since the camera mount has a 1X lens, the NA is the same at the camera plane as at the intermediate image plane.

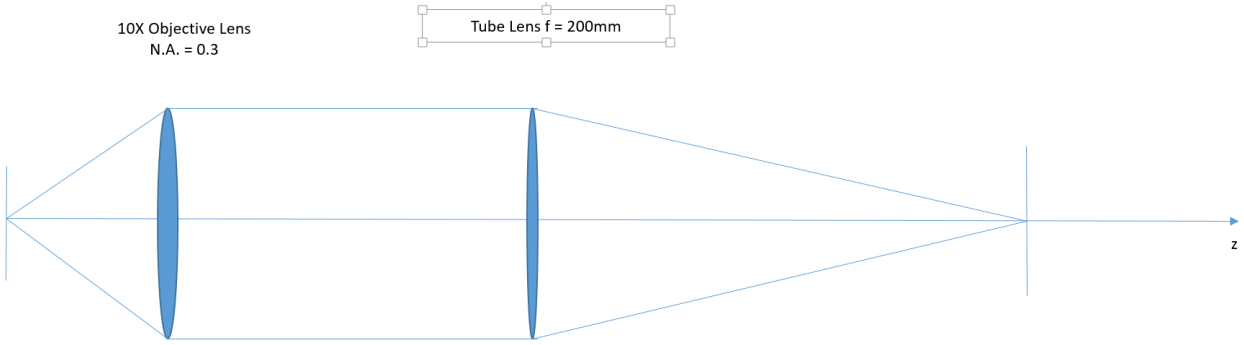

Figure 3.2. The lateral magnification of the objective lens and tube lens to acquire the N.A. in image space

To determine NA of the confocal microendoscope in image space, the magnification is given as the ratio of the focal lengths between the Olympus 10X objective (f_{obj} = 18mm) lens. The NA of the objective lens divided by the magnification, gives an image space NA of 0.054.

3.1.4 Transmission Calculation

As mentioned in the beginning of section 3.1.2, we want to compare expected imaging performance with the fluorescence microscope and the confocal microendoscope. An important difference between the two is the reduced optical transmission of the confocal microendoscope. In performing this calculation, we assign the value of the transmission coefficient of the fluorescence microscope to be equal to 1 since we are looking at relative optical throughput. The digital signal readout (S) of a detector is given as

$$S = N_e * CF, \tag{3.8}$$

where N_e is the number of photoelectrons produced, and CF is a conversion factor. CF is described as the ratio of the max digital readout S_{full} to the full-well capacity (FWC) divided by the gain FWC/G. Hence,

$$CF = \frac{S_{full}}{FWC} G. \tag{3.9}$$

The number of photoelectrons generated in a detector pixel is equal to the number of photons incident on the detector pixel times the quantum efficiency for conversion of photons to photoelectrons,

$$N_e = N_p * QE. \tag{3.10}$$

The number of photons hitting a detector pixel is the incident energy E on the detector pixel divided by the energy per photon. For monochromatic light, this is given by,

$$N_p = \frac{E}{h*v}, \tag{3.11}$$

where h is plank's constant and v is the frequency of the incident photons. For a narrow band of frequencies, the average frequency v can be used as a good approximation. Now taking equations (3.7 – 3.11) and substituting them into equation 3.8, we get the following expression for the digital signal S out of the camera,

$$S = \frac{I_{img}*A_{pixel}*t_{ex}}{h*v} * QE * \frac{D_{full}}{FWC} * G. \tag{3.12}$$

Combining equation (3.2) into equation 3.12, the signal expression becomes,

$$S = \frac{L_{img}*\Omega*A_{pixel}t_{ex}}{h*v} * QE * \frac{D_{full}}{FWC} * G. \tag{3.13}$$

With equation (3.1) the signal expression becomes,

$$S = \frac{L_{obj}*T*\Omega*A_{pixel}t_{ex}}{h*v} * QE * \frac{D_{full}}{FWC} * G. \quad (3.14)$$

Our goal is to compare the relative transmission coefficient of our confocal microendoscope (T_C) with respect to the Nikon system. If we assume a transmission coefficient of our Nikon system ($T_N = 1$), the ratio of signals obtained with the two systems can be used to determine T_C.

$$\frac{S_N}{S_C} = \frac{\frac{L_{objN}*T_N*\Omega_N*A_{pixelN}*t_{exN}}{h*v}*QE_N*(\frac{D_{full}}{FWC})_N*G_N}{\frac{L_{objC}*T_C*\Omega_C*A_{pixelC}*t_{exC}}{h*v}*QE_C*(\frac{D_{full}}{FWC})_C*G_C}, \quad (3.15)$$

where, the subscripts N and C refer to the Nikon E600 imaging system and the confocal imaging system, respectively. The last factor we have to take into consideration is the fluorescence emission radiance in object space (L), which is proportional to the irradiance of the excitation (I_{ex}) times the molar extinction coefficient of the fluorophore (ε) times the concentration of the fluorophore (C) times its fluorescence quantum yield (η). We measured the incident power onto our object, as mentioned earlier. Therefore, the excitation irradiance can be obtained by the measured power divided by the cross-sectional area of the illuminated field-of-view (FOV) of both systems in tissue space. For the Nikon system, the FOV in tissue space is related to the field number divided by the lateral magnification. The field number is 22, and the objective used was a 10X objective, giving a FOV diameter of 2.2mm. For the confocal system, the FOV in tissue space corresponds to the fiber bundle diameter divided by the magnification of the miniature objective lens, which in this case is 0.450mm. The illuminated areas come out to be, 3.8mm^2 for the Nikon

and 0.16mm^2 for the confocal system. Substituting the excitation irradiance, extinction coefficient, molar concentration and quantum yield, our expression is

$$\frac{S_N}{S_C} = \frac{\frac{I_N * T_N * \varepsilon * C * \eta * \Omega_N * A_{pixelN} * t_{exN}}{h\nu} * QE_N * (\frac{D_{full}}{FWC})_N * G_N}{\frac{I_C * T_C * \varepsilon * C * \eta * \Omega_C * A_{pixelC} * t_{exC}}{h\nu} * QE_C * (\frac{D_{full}}{FWC})_C * G_C}. \quad (3.16)$$

The object used for our measurements was the same for both systems. In this case, the factors ε, C and η cancel out. Other factors that cancel out or that were set equal for this measurement include the energy for the incident photons on our detector (hv), as well as, the system gains and integration times. So our final expression for the relative optical transmission calculation assumes the form,

$$\frac{T_C}{T_N} = \frac{S_C * I_N * \Omega_N * A_{pixelN} * QE_N * (\frac{D_{full}}{FWC})_N * G_N}{S_N * I_C * \Omega_C * A_{pixelC} * QE_C * (\frac{D_{full}}{FWC})_C * G_C}. \quad (3.17)$$

The calculation for T_C with the necessary parameters was performed in a Matlab program.

Table (3.1) shows the parameter values for both systems and table (3.2) shows the calculated results. Regarding the process of computing the number of photoelectrons produced, we used the following expression,

$$N_e = \left(\frac{S_R - S_B}{S_{Full}}\right) * \left(\frac{1}{G} * FWC\right). \quad (3.19)$$

Equation 3.19 is the re-arranged form of equation (3.8). Once the number of photoelectrons is computed for a given digital signal, we invoke equation (3.10) to obtain the number of incident photons.

The signal-to-noise ratio can be calculated from the ratio of the average signal minus the background signal (no light situation), to the standard deviation of the background signals.

$$SNR = \frac{\langle S_R \rangle - \langle S_B \rangle}{\sigma_B}, \tag{3.20}$$

where $\langle S_R \rangle$ is the average fluorescent signal, $\langle S_B \rangle$ is the average background signal, and σ_B is the standard deviation of the background signal. The standard deviation of background signal is primarily attributed to the read noise of the detector. Although we limited noise sources to read noise for our calculation, it is not the only form of noise present. There is noise attributed to dark current and noise attributed to incident photons. However, these noise sources were considered to be small relative to the camera read noise at the short integration times and low signal levels of the acquired images.

	Nikon	Confocal
Excitation Irradiance(mW/mm^2)	1.3153	8.1739
Pixel Area (μm^2)	182.25	28.09
Integration Time (msec)	30	30
QE at 810 nm	.74	.47
S_{Full}	65,536	1024
Full Well Capacity (e$^-$)	100,000	8,400
Gain	4	4
Average Signal	9223	258
Average Background Signal	2000	12
Standard Deviation	16	4.3

Table 3.1. Measured parameters for transmission calculation

	Nikon	Confocal
Transmission Coefficient	1	0.096
N_e	2755	504
N_p	3723	1073
SNR	451	57

Table 3.2. Calculated parameters for transmission calculation

The calculated relative optical throughput for the confocal system was estimated to be about 10% of the Nikon system. The confocal system loses about 50% of the light transmitting in one direction through the fiber-optic bundle. It loses considerably more light with the presence of the confocal slit, and with more optical components. This result is roughly in the right ballpark as to what is expected. The ratio of the calculated signal to noise ratios is about a factor of 7.9.

Chapter 4 Experiments, Data and Results

Introduction

A number of experiments were conducted to determine the feasibility of using a fluorescence optical imaging system for flow cytometry and eventually for in vivo applications. We used a piece of tissue paper on a slide, stained with a fluorescent contrast agent OTL 38. We performed a number of in vitro experiments. We imaged OVCAR3 cells labeled with OTL38. Other experiments were performed to compare transmission and detection levels with three optical system configurations: the Nikon Eclipse E600 fluorescence microscope with the PIXIS 2048B, the Nikon Eclipse E600 with the DCC 3240N, and the custom confocal microendoscope. Imaging was done with fluorescently labeled PDX breast cancer cells with OTL 38 in various in vitro setups. Setups involved imaging PDX breast cancer cells on a slide. We also compared PDX cells to immortalized MCF10A cells. Simulations of vasculature were performed by placing PDX cells in capillary tubes. Also, we performed a simulation of a vasculature flow mechanism with fluorescent microspheres by inserting the spheres into a square capillary tube and moved the tube through the FOV on a translational stage. The results presented will be placed in two categories: phantom setups; and imaging of cells.

4.1 Non-Cellular and Phantom Experiments

4.1.1 Confocal Microendoscope with Stained OTL38 Tissue Paper

We used OTL38 stained tissue paper to qualitatively examine the detection capabilities of the confocal microendoscope.

We performed initial experiments by taking images with the confocal microendoscope of tissue paper stained with OTL38. We prepared two solutions of OTL38 at a dilution ratio of .05mL OTL38/.5mL saline and .05mL OTL38/5mL saline. We stained a piece of tissue paper with the diluted contrast agents and analyzed the images acquired at an integration time of 30msec. The samples were illuminated with a 780 nm laser. Figure (4.1) shows the images collected.

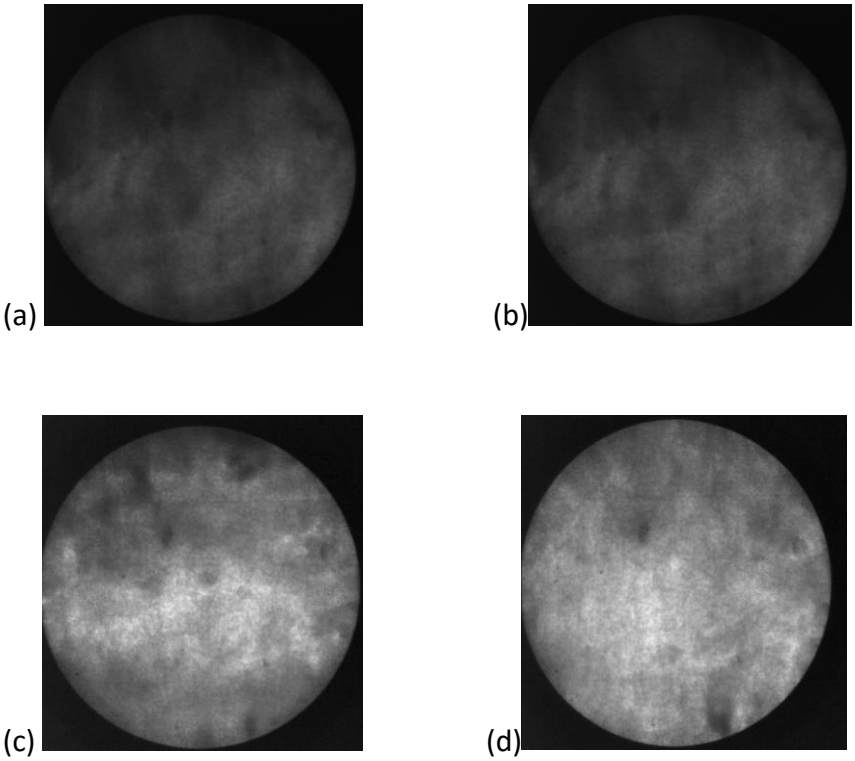

Figure 4.1. Images of OTL38 stained tissue paper. (a-b) have a dilution ratio of .05/.5mL and (c-d) have .05mL/5mL

The average signal between the two images acquired for the 10:1 dilution ratio was 343, and the average signal between the two images for the 100:1 dilution ratio was 38. The results indicate that for a decrease on the dilution ratio from 100:1 to 10:1 of PBS to OTL38, there is an increase in signal by approximately a factor of 9. Since the two dilution ratios are different by a factor of 10, we would expect the factor of signal to increase proportionally to the decreased dilution ratio.

4.1.2 Quantitative Phantom Experiment Microsphere Flow Cytometry Experiment

We used microspheres and square crit tubes to demostrate that we could see objects of approximately the size of cells. We used square crit tubes to avoid having to immerse the tubes in water in order to correct for astigmatism in light traversing an object with significance cylindrical shaped index of refraction variation. We used 15µm diameter polystyrene microspheres that fluoresce at an excitation wavelength of 505 – 515 nm. We used the G-2A cube, which has a 510-560 nm excitation band, a dichroic wavelength of 565 nm, and a 575 nm long pass filter with a bandwidth of 75 nm [16]. In preparing the phantom, we used a 10:1 dilution ratio of PBS to sphere solution to obtain a relatively sparse distribution of microspheres in order to emulate the conditions present for rare CTCs. This diluted solution was drawn into the crit tube, and placed on a translation stage. Lateral motion of the translation stage emulated flow of cells through the FOV. The Nikon Eclipse E600 fluorescent microscope was used, along with both the PIXIS 2048B CCD and ThorLabs DCC 3240N CMOS cameras. Static test images were taken with the PIXIS camera; and videos were taken with faster frame rates with the ThorLabs DCC 3240N.For the test images, we used a 10X/0.3 objective. The PIXIS was set to an integration time

of 30 msec. Figure (4.2) shows examples of the test images from the PIXIS with different illumination powers and gain conditions.

The goal was to create a range of excitation illumination in an attempt to establish the minimum detection capacity of both camera systems of the fluorescent signals.

(a) 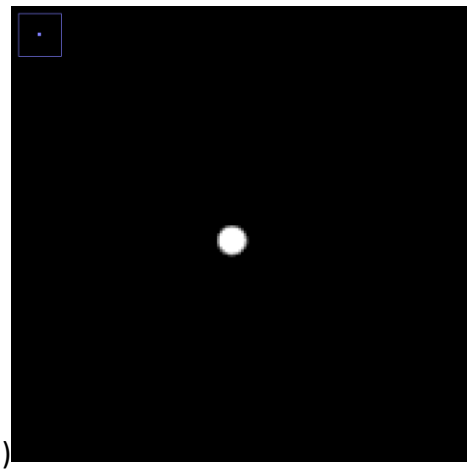 (b) 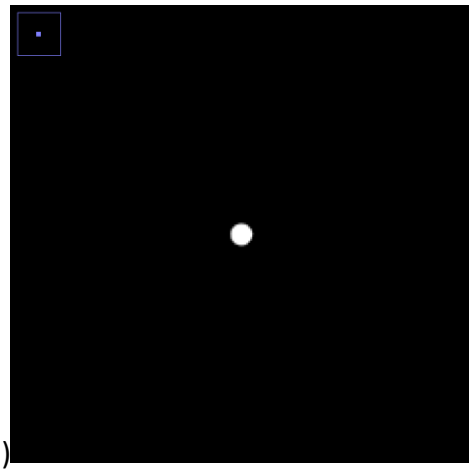

(c) 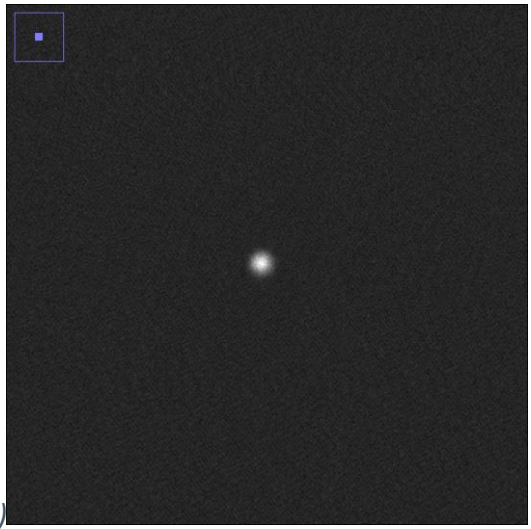

Figure 4.2. These are three test images taken from the PIXIS 2048B depicting fluorescent microspheres. (a) Image taken with the ND-16 filter and a gain of 1. (b) Image taken with the ND-16 and a gain of 4. (c) Image taken with the ND4, ND8, and ND16 filters in and a gain of 1

Videos were collected with the DCC 3240N using the software ThorCam. Figure (4.3) shows four still frames collected from one of the videos with the ND4, ND8 and ND16 filters in the illumination path. All the videos taken were at 30 images per second, a gain of 4, and 100 total frames. The first video used the ND16 filter, the second video used both the ND16 and ND8 filters, and the third video used all three filters. After all the data were collected, quantitative analysis was performed in which calculations of SNR, number of electrons, and number of photons were done. Table (4.1) shows the quantitative analysis.

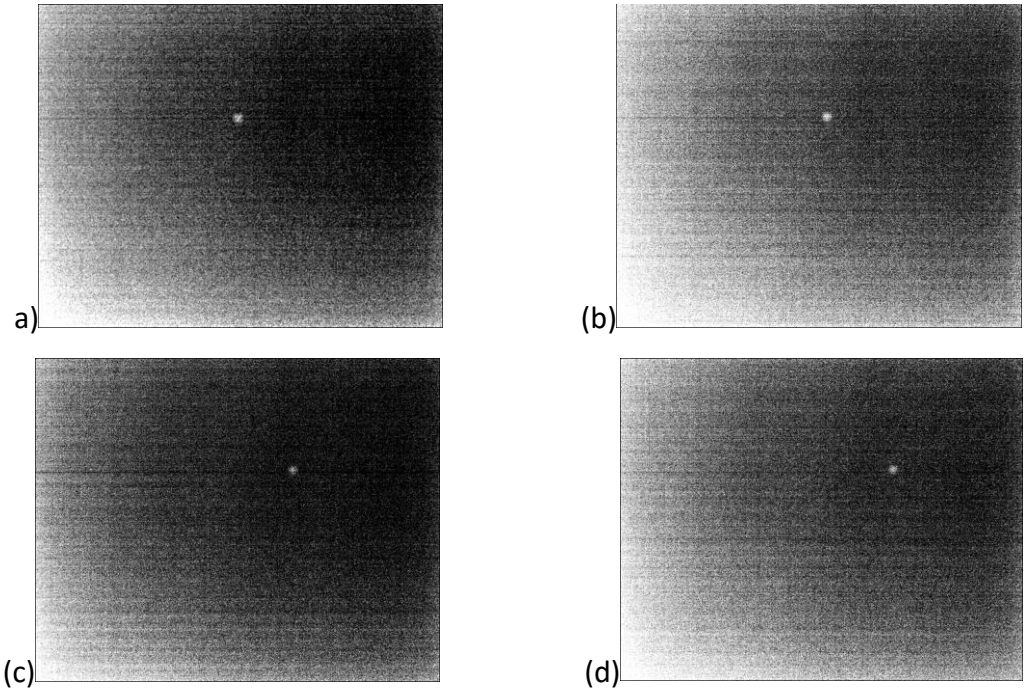

Figure 4.3 (a-d). These images show a microsphere moving through the FOV as a translational stage is being moved using the Thor DCC 3240N camera with all the ND4 ND8 and ND16 filters with an SNR of 2.3.

Camera	Objective	t_i	ND	Gain	S_a	S_b	Standard Deviation	SNR	N_e	N_p
PIXIS	10X	30msec	16	1	3362	664	4.2	642	4117	4334
PIXIS	10X	30msec	16	4	11,881	2000	16	617	3769	3967
PIXIS	10X	30msec	16,8,4	1	787	664	4.2	29	187	197
Thor	10X	30msec	16	4	288	82	5.6	37	422	602
Thor	10X	30msec	16,8	4	116	82	5.6	6	70	99
Thor	10X	30msec	16,8,4	4	95	82	5.6	2.3	27	38

Table 4.1. Results of microsphere experiment. Lowest SNR = 2.3 on the Nikon/Thor system with ND4 ND8 and ND16 filters in place.

The SNR ratios experimentally measured between row 2 divided by row 4 was 16.7. The predicted results for SNR ratios between the Nikon/PIXIS and Nikon/Thor configurations was estimated to be 19.3 (shown in section 4.2.3). There is an inconsistency here due to a source of error in the predicted calculation due to a different imaged object for rows 2 and 4. The minimum SNR recorded from the PIXIS images was 29. However, upon further examination of the image that yielded this result, there were cells in the FOV that appeared dimmer in signal, so it is possible to resolve objects in our image that yield a lower SNR. The lowest SNR yielded from the DCC 3240N was 2.3. It is important to note that we were able to qualitatively resolve the microsphere present in the field of view with this level of SNR as shown in figure (4.3). We felt that this level established a threshold for the minimum SNR that can be detected with the Nikon E600 and the ThorLabs DCC 3240N camera. It is conceivable that we will be able to see cells in the NIR region should they yield an SNR of around the same level with this imaging system.

4.2 Cell Experiments

4.2.1 Quantitative Analysis with Labeled OVCAR3 Cells with OTL38

For this experiment, we used OTL38 labeled OVCAR3 ovarian cancer cells, and imaged them under the Nikon Eclipse E600 microscope with a TE/CCD 512FT camera system made by Princeton Instruments. The camera detector is 512 X 512 pixels with each pixel size of 15 µm X 15 µm. The TE/CCD 512FT has a scan rate of 512MHz, a full well capacity of 200,000e^-. It has a quantum efficiency of ~40% at 810nm [17]. This served as a first test to see how well we could see fluorescently labeled tumor cells in the NIR spectrum with the Nikon microscope. Most ovarian cancer cells overexpress folate-receptor, and we wanted to evaluate the cellular uptake of OTL38.

This procedure involved OVCAR3 cells grown on a glass cover-slip. We incubated the cells for one hour in 0.25mL of media added to 0.25mL of 0.05mL/0.5mL of OTL38/PBS solution. The coverslips were then rinsed and placed upside down on a microscope slide. We took four images of the prepared sample. Three of the images were taken using a 20X 0.75 NA objective, and one of the images was taken using a 10X 0.3 NA objective. The images were acquired with an integration time of 20 seconds, which was needed to obtain sufficient signal. We used an ICG cube for illumination. The cube has an excitation spectrum of 748-789 nm, an emission wavelength of 810-851 nm, and a dichroic wavelength of 801 nm. Figure (4.4a) shows the image with the 10X objective lens, and figures (4.4b-4.4d) show the images acquired with the 20X objective.

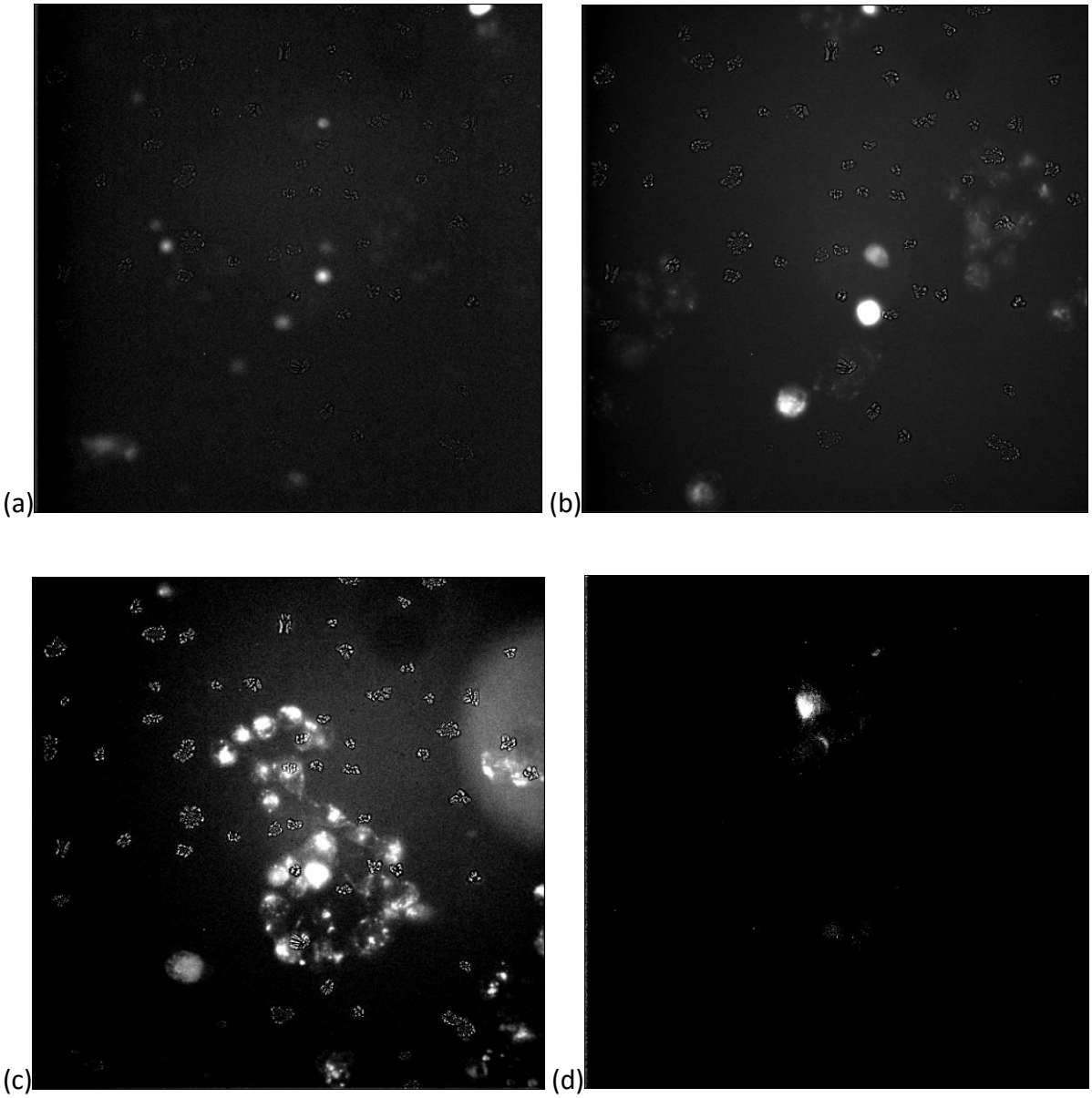

Figure 4.4. Images of the OVCAR3 cells with the Nikon with a TE/CCD 512FT camera. (a)Image of OVCAR3 cells using a 10X objective. (b-d) Images of OVCAR 3 cells using 20X objective lenses

Even with the long integration time of 20 sec, we experienced low signal levels in our images. The average background subtracted signal from all four images was measured to be about 1824, and the background signal was 1430 with a standard deviation of 13.4. The SNR for the average signals was calculated to be 29.4. For flow cytometry, a more reasonable integration time would be 30msec. The average background subtracted signal divided by a factor of 667 to

account for the signal conversion from 20 sec to 30msec, we get 0.59. The SNR obtained from this background subtracted signal is 0.04. We would not be able to detect fluorescent signal with this SNR. This is possibly due to poor uptake of the contrast agent by these OVCAR3 cells. Other reasons might have involved too short of an incubation period, or insufficient rocking of the container to allow for adequate distribution of the contrast agent over the cells. Regardless, as we will see in later experiments, the uptake of the contrast agent OTL38 by the OVCAR3 cells was not very good and clearly inadequate for real-time in vivo flow cytometry.

4.2.2 Sensitivity Test with PDX and Immortalized Cells with OTL38 and Nikon Microscope

The purpose of this experiment was to investigate cellular uptake and fluorescent signals acquired by labeling PDX breast cancer cells with OTL 38. These PDX breast cancer cells were derived from patient breast cancer tissue in Dr. Ghassan Mouneimne's lab in the University of Arizona Cancer Center. We used a non-cancerous breast cell, MCF10A, as a negative control since this cell line does not have a high expression of folate receptor. The test of PDX breast cancer and immortalized (MCF10A) cells involved analyzing the two types of cells under two growth conditions: PDX and immortalized cells growing on a glass coverslip, and both cells types growing on a layered gel substrate. The latter was of particular interest to the Mouneimne lab. The optical system employed for this experiment was the Nikon Eclipse E600, with the PIXIS 2048B CCD camera system. Both cell types were received on the substrates in multi-well plates immersed in growth media. We incubated two cell cultures of both cell lines. The first cell culture was incubated for about one hour in .05mL of OTL38 to .5mL of PBS. The second cell culture was incubated for about two hours in the same dilution ratio of OTL38.

Images of the first cell culture were obtained using the 10X 0.3NA objective with integration times of 30 msec and 100msec. After imaging the PDX cells, we followed the same procedure with the MCF10A cells but with 10 sec and 100 msec integration times. Figure (4.5) shows the results.

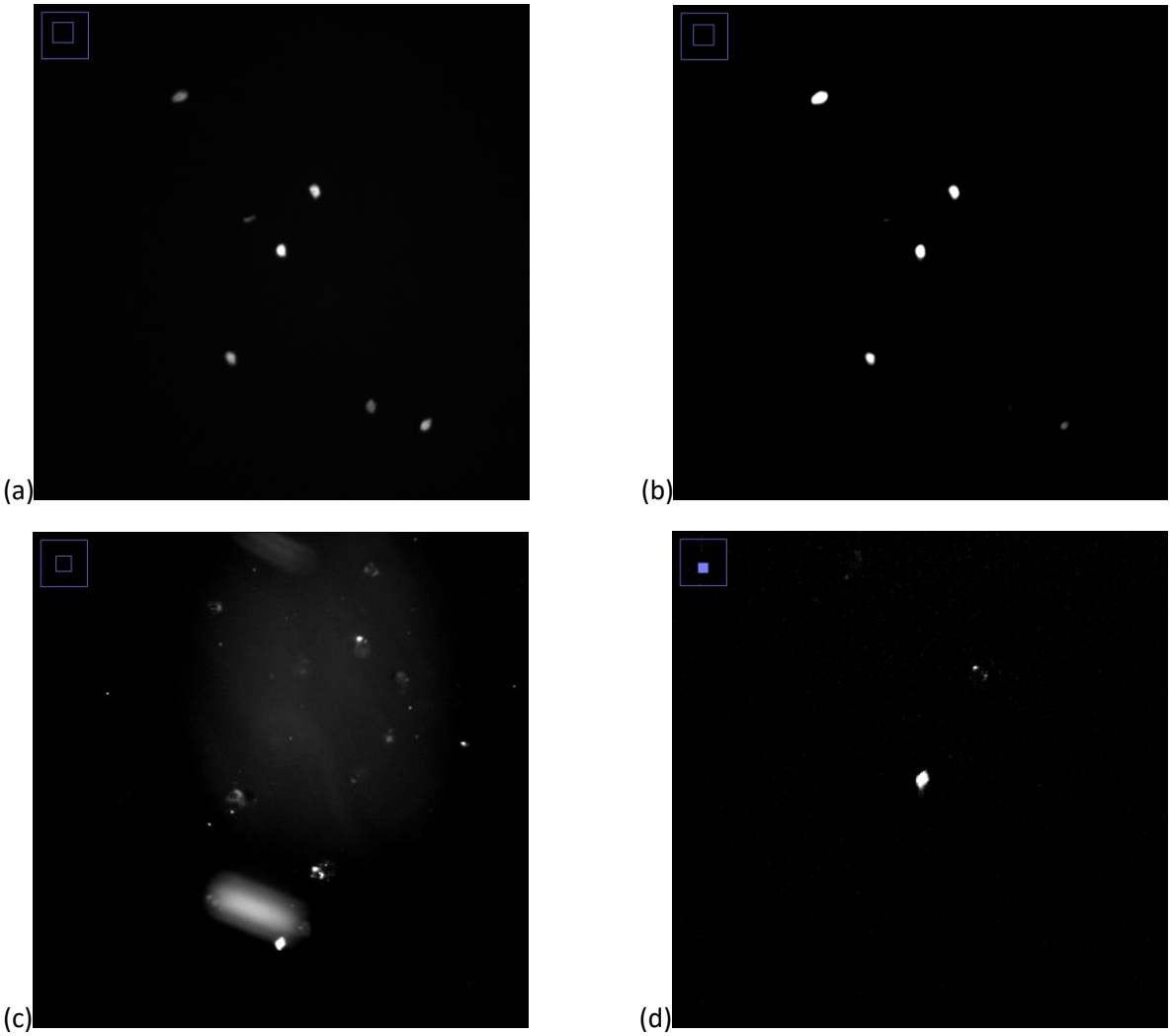

Figure 4.5. Images of PDX and MCF10A cells from cell culture 1 with a 10X objective. (a) PDX cancer cells with an integration time of 30msec. (b) PDX cancer cells with an integration time of 100msec. (c) MCF10A cells with an integration time of 10sec. (d) MCF10A cells with an integration time of 100msec.

We took images of the second cell culture using a 10X 0.3NA water immersed objective lens, and acquired images directly from each well, as opposed to taking the coverslip out and

placing them on a slide. This process was performed to see if we would get better images by not having to repeatedly wash the coverslips. All of these images were acquired with an integration time of 100 msec.

Qualitatively, we recognize that the signals from the PDX cells are higher than those produced by the MCF10A cells. Moreover, the signals for cell culture 1 were higher than signals in cell culture 2.

After the images were collected, an analysis was carried out for each image in which we calculated: the number of photoelectrons, the number of incident photons, and the SNR, using the equations from section 3.3, as can be shown in table (4.2)

Cell Type	Objective	t_i	S_a	S_b	Standard Deviation	SNR	N_e	N_p
PDX	10X	30msec	6534	1986	16	284	1735	2344
PDX	10X	100msec	23,888	1986	16	1369	8355	11290
MCF10A	10X	10sec	13,896	1986	16	660	4543	6140
MCF10A	10X	100msec	2440	1986	16	28	173	234
PDX	10XW	100msec	3345	1986	16	80	518	701
MCF10A	10XW	100msec	2225	1986	16	10	91	123

Table 4.2. Quantitative results of PDX cancer cells and MCF10A cells for cell culture 1 and cell culture 2. Rows 1-4 pertain to cell culture 1. The last two rows pertain to cell culture 2 with the use of a water-immersed objective lens.

What could be concluded from the experiments is that the higher signals for the PDX cells versus the MCF10A cells is due to the higher efficiency of the cell line's ability to uptake the fluorescent conjugate. The MCF10A cell line had a very low uptake of the fluorescent agent, and as a result, signal was very low. The SNRs analyzed for the first cell culture were generally higher than the signals in the second cell culture. There are multiple factors that may account for the

lower signals. The first factor could be attributed to internalization. This is a time-dependent process in which a ligand breaks off of the receptor site on the cell's membrane [18]. A second factor that may have affected the results is the use of the water-immersion objective and imaging cells immersed in fluid directly in the well. It is also unclear whether the signals we were reading were pertaining to cells. Another possible factor to consider was both cell cultures tested positive for mycoplasma. This is a bacteria that produces a P1 antigen that allows adhesion to epithelial cells [19]. It's unclear whether this may have hindered the binding process of OTL38 to folate-receptor sites.

4.2.3 PDX Cells in Capillary Tube

In another experiment, we put OTL38 labelled PDX cancer cells into a cylindrical capillary tube. The purpose of this experiment was to image cells in an environment that simulates the conditions of a superficial capillary vessel in the oral mucosa, which is located just beneath the inner surface of the lip. This involved imaging cells in a capillary tube with the Nikon Eclipse E600 microscope, quantifying the signal levels and SNR, and estimating based on theoretical sensitivities what the SNR would be with the ThorLabs camera, which can operate at video rates, or the confocal system. Since it was damaged, the confocal microendoscope could not be used for this experiment. We did look to confirm results in a later experiment with the confocal microendoscope. The experimental procedure was a little different than in previous experiments. For this experiment, trypsin was used to break down proteins on the cells surfaces, which enabled them to be released from the glass substrate into the surrounding media so that they can be inserted into the capillary tube. We prepared a 10:1 diluted solution of OTL38 with .05mL of OTL38 and .5mL of PBS. We then took 250 µL of the diluted OTL 38 and combined it with 500 µL

of media, which was inserted into each well of the multiwell plate. We then placed the cells on a heating pad and incubated them for one hour. After the incubation process, we extracted the coverslips, and rinsed them with PBS. We placed the coverslip back in a well, used 1000µL of trypsin to release the cells from the coverslip, and centrifuged the resulting solution for 5 minutes to separate the cells from the trypsin. We extracted most of the trypsin from the vial, and refilled the vial with 500 µL of PBS. We then proceeded to centrifuge again for 30 seconds, and replenished the vial with another 500 µL of PBS. We then placed the vial onto a vortexer in order to resuspend the cells. The capillary tube was then inserted into the vial to fill the tube with OTL-labelled cells suspended in PBS.

To correct for effects caused by the cylindrical lens, we submerged the cylindrical capillary tube containing the OTL-labelled cells in water. This enabled better matching of refractive indices which corrected the aberrations (primarily astigmatism of the cylindrical glass geometry). Data were collected for the aberration corrected images. Images were acquired with the PIXIS 2048B CCD camera, a 10X 0.3NA objective, and with a 100 msec integration time. Figure (4.6) shows some of the images collected.

(a) 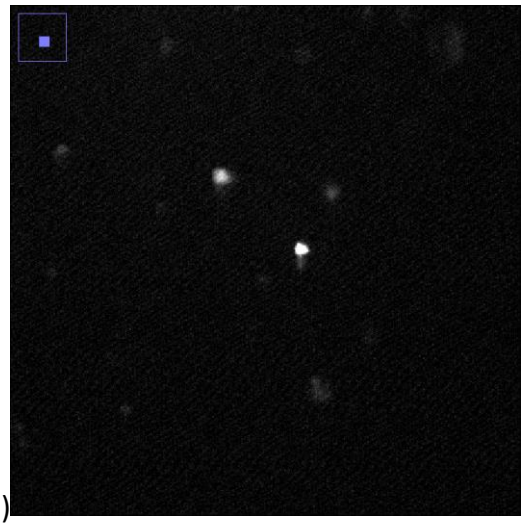 (b) 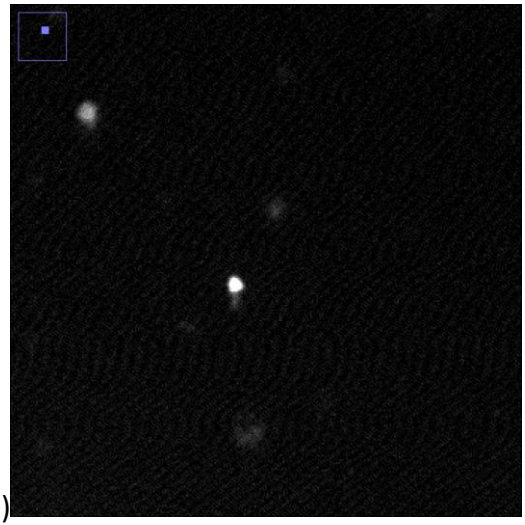

Figure 4.6 (a-b). Images of OTL38-labelled PDX cancer cells in a capillary tube submerged in water with a 10X objective and a 100msec integration time with the Nikon/PIXIS

The signals observed in this experiment were considerably lower than what was experienced in the first cell culture of the previous experiment. The average background-subtracted signal was 580 as opposed to 21902 from the previous experiment with an integration time of 100msec. The average SNR for the cells in these images was 36.3, the average number of photoelectrons was 221.3, and the average number of photons was 299. These results indicate that both the signals and cellular uptake of OTL38 were relatively low. The aspects of this experiment that remained constant were the cells and the dilution ratio of OTL38. What did not remain constant was the introduction of trypsin. It's concievable that the trypsin may have hindered the ability for OTL38 to remain bound to the cell surface, due to the breakdown of protein structures, residing on the cell surface. Moreover, the uptake of the OTL38 may have also been hindered by an infected cell line due to the presence of mycoplasma. It is also possible that we were not observing cells, since there was no control in place to positively identify cells.

Using the highest and lowest SNR data parameters acquired from the original data set for 100msec integration times of the Nikon/PIXIS, these data served as a good range to compare the

three system configurations. In performing these predicted calculations, the two data parameters were scaled down for 30 msec integration times. The values for background subtracted signals, SNR, N_e, and N_p for the confocal microendoscope with the ThorLabs DCC 3240N camera system were estimated. We did this using the known parameters and calculated transmission value of the confocal system. We also calculated thoeretical results for the Nikon system using the same DCC 3240N camera system rather than the PIXIS 2048B CCD camera. Table (4.3) shows the theortical SNR calculations for the confocal microendoscope and the Nikon system with the DCC3240N camera, as well as, the SNR between all three systems. These data values are based on the assumption of a gain of 4 for the DCC 3240N, as well as a 30 msec integration time.

System	Cell Type	Objective	t_i(msec)	S_a-S_b	Gain	Standard Deviation	SNR	N_e	N_p
Nikon/PIXIS	PDX	10X	30	69	4	16	4.3	26	36
Nikon/PIXIS	PDX	10X	30	287	4	16	18	109	147
				Predicted Results					
Nikon/Thor	PDX	10X	30	1.26	4	5.6	0.22	3	5.5
Nikon/Thor	PDX	10X	30	5.26	4	5.6	0.93	11	23
Confocal	PDX	10X	30	2.55	4	4.3	0.59	5	11
Confocal	PDX	10X	30	10.1	4	4.3	2.3	21	44

Table 4.3. Results for predicted data and system comparisons. Rows 2,4, and 6 were used for SNR comparisons. For the highest data points the SNR ratio between Nikon/PIXIS and confocal is 7.8. The SNR ratio between the confocal and the Nikon/Thor is 2.5. The SNR ratio between the Nikon/PIXIS and Nikon/Thor is 19.3

When analyzing the data sets of Table(4.6), we notice that the SNR ratio between the Nikon/PIXIS and the confocal system is 7.8. We calculated the SNR ratio to be 7.9 in the previous chapter for the system throughput analysis test. The source of error is attributed to one result pertaining to a theoretical calculation of signal and the other result pertaining to direct

experimental measurements of signal to calculate the relative optical system throughput. The SNR ratios between the confocal versus the Nikon/Thor and the Nikon/PIXIS versus the Nikon/Thor are 2.5 and 19.3 respectively. It is predicted that the confocal system will yield a slightly higher singal and SNR than the Nikon system, with the ThorLabs DCC 3240N camera, a 10X 0.3NA objective, and the same integration time. Despite the significantly lower relative transmission of light, the confocal system yields a higher SNR than the Nikon system, when both systems use the DCC3240N. This is due to the confocal system having a higher NA in image space NA = 0.054, as opposed to an NA = 0.03 on the Nikon system using a 10X objective. The next experiment will show results acquired from all three system configurations, imaging OTL38-labelled PDX cells on a slide with a glass cover-slip.

4.2.4 Imaging of PDX Cells with Three System Configurations

In section 4.2.3, we showed thoeretical predictions for the SNR of cell images for both the confocal system and the Nikon system mated to the ThorLabs DCC 3240N camera. These results were calculated using the equations derived in section 3.1.4 and the experimental data obtained from the Nikon system mated to the PIXIS 2048B camera. The current experiment involves collecting images of OTL38-labeled cancer cells with the three system configurations and measuring quantitative parameters, including SNR, number of photoelectrons, and the number of photons. We prepared a 10:1 dilution ratio of OTL38 with saline (.05ml OTL38/.5ml saline). The cells were grown on a glass coverslip in growth media. Before incubating with the OTL38, we collected a brightfield test image to identify cells. This image was acquired with the PIXIS 2048B, using a 20X/0.75 objective, and 100msec integration time.

For the incubation procedure, we extracted the media from two wells and inserted 360 µL of OTL38 into both wells. We allowed well 1 to incubate for one hour, and we allowed well 2 to incubate for 2 hours. After which, we performed a rinse with PBS solution and flipped the coverslip over onto a slide for imaging. A second brightfield test image was conducted with the same system parameters as can be shown in figure(4.7).

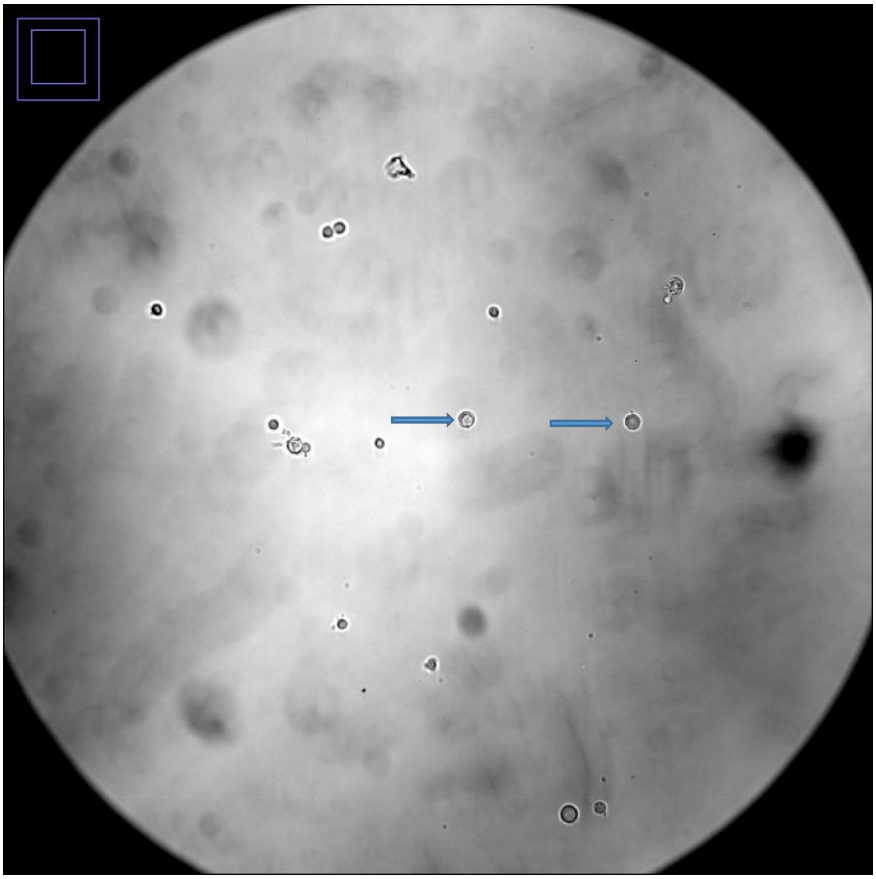

Figure 4.7. Second brightfield test with OTL38 and after rinse. The arrows indicate cells in the image.

We noticed that there were fewer cells observed compared to what we saw before rinsing. After acquiring test images, we proceeded to acquiring fluorescence images with well 1, using the Nikon-PIXIS and Nikon-ThorLab camera configurations. We employed the same 20X

objective lens and used both 30msec and 100msec integration times. Both camera systems were set to a gain of 4. Figure (4.8) shows images from both the PIXIS and ThorLab cameras and Table (4.4) shows the quantitative data for well 1. The signals depicted are the background subtracted signals.

(a) 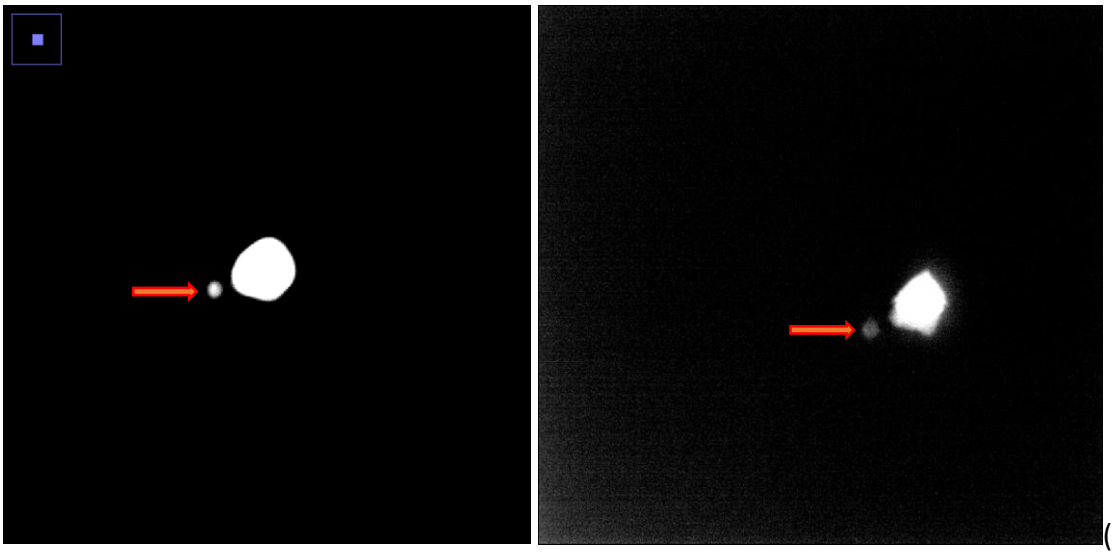 (b)

Figure 4.8 (a-b). Images of OTL38-labeled PDX cells taken from the Nikon system using the PIXIS 2048B and ThorLabs DCC3240N from well 1. Arrows indicate the object measured for signal. The larger bright spot in both images yielded a suspicious shape, and was questionable as to whether or not it is a cell.

.

System	Cell Type	Objective	t_i(msec)	S_a-S_b	S_b	Gain	St. Deviation	SNR	N_e	
Nikon/PIXIS	PDX	20X	30	9221	1928	4	16	576	3517	4752
Nikon/PIXIS	PDX	20X	30	17,417	1928	4	16	1088	6644	8798
Nikon/PIXIS	PDX	20X	30	16,105	1928	4	16	1006	6143	8302
Nikon/PIXIS	PDX	20X	100	7261	1928	4	16	454	2769	3743
Nikon/PIXIS	PDX	20X	100	1321	1928	4	16	83	504	681
Nikon/Thor	PDX	20X	30	185	235	4	5.6	33	379	807

Table 4.4. Quantitate Results for well 1 for a 1 hour incubation time.

The incubation period in well 2 was extended to two hours. We performed a rinse with PBS and flipped the coverslip onto a slide for imaging. A second brightfield image using the Nikon/PIXIS was taken along with a complimentary fluorescent image, as can be seen in figure (4.9). A 20X objective was used with an integration time of 30msec for image acquisition.

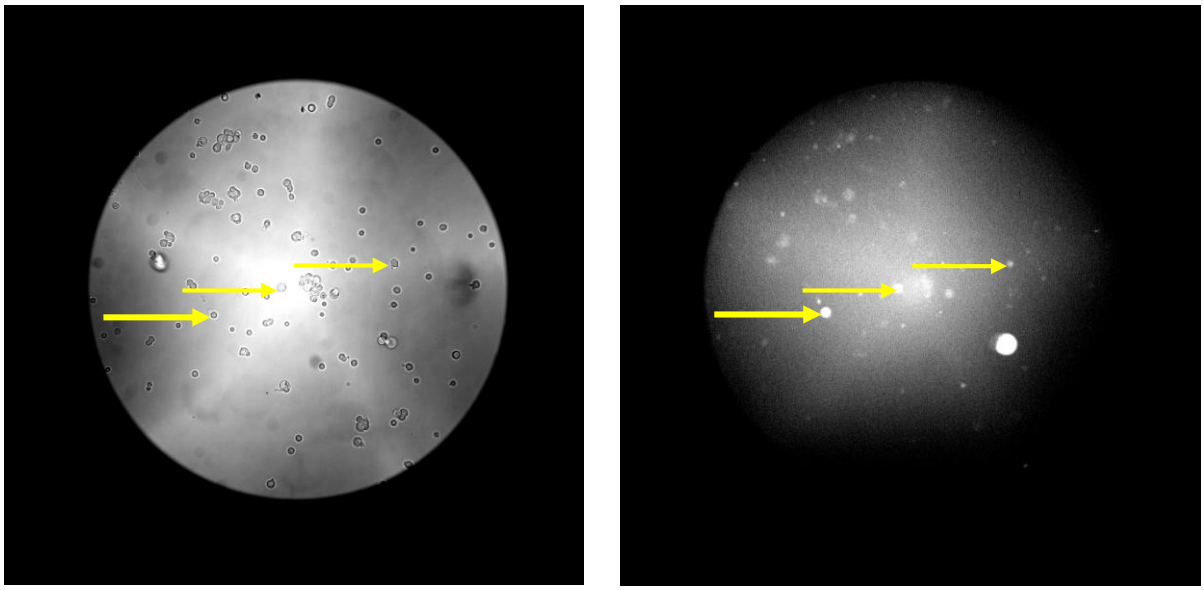

Figure 4.9 (a-b). Brightfield image and corresponding fluorescent image of PDX cells with Nikon/PIXIS system from well 2. The three arrows indicate cells that were identified and measured. The background subtracted signal from the left arrow is equal to 1499 with an SNR of 94. The signal from the cell at the center arrow was 580 with an SNR of 36. The signal from the cell at the right arrow was measured at 408 with an SNR of 26.

We observed that the number of cells from well 2 in the brightfield image was greater than well 1. The cells in the brightfield image were identified in our fluorescent image, and we took measurements of the fluorescent signals of each cell. We proceeded to collect images from the same slide on the Nikon/PIXIS, Nikon/Thor, and Confocal/Thor systems. However, we were not able to register the images to measure the same cells on the three systems. Integration times and gains were set with all systems at 30msec and a gain of 4. It is important to note that the

confocal system was running on autoscale mode. This alters the gain and enhances both background signals and standard deviation. Table (4.5) shows the experimental results of well 2.

System	Cell Type	Objective	t_i(msec)	S_a-S_b	S_b	Gain	St. Deviation	SNR	N_e	N_p
Nikon/PIXIS	PDX	10X	30	1390	1928	4	16	87	530	717
Nikon/PIXIS	PDX	10X	30	1626	1928	4	16	102	620	838
Nikon/PIXIS	PDX	10X	30	2182	1928	4	16	136	832	1124
Nikon/PIXIS	PDX	10X	30	1430	1928	4	16	89	545	737
Nikon/PIXIS	PDX	20X	30	1499	1928	4	16	94	572	773
Nikon/Thor	PDX	10X	30	17	235	4	5.6	3	35	74
Confocal	PDX	10X	30	136	152	4	20	6.8	279	593
Confocal	PDX	10X	30	56	152	4	20	2.8	115	245
Confocal	PDX	10X	30	132	152	4	20	6.6	270	574
Confocal	PDX	10X	30	264	152	4	20	13.2	541	1152

Table 4.5. Results for well 2. Rows 2, 6, and 7 were selected from each system to compare SNRs. SNR ratio for Nikon/PIXIS vs. confocal is 15. SNR ratio for confocal vs. Nikon/Thor is 2.3. SNR ratio for Nikon/PIXIS vs. Nikon/Thor is 34.

When analyzing these data, it was apparent that the number of adequately labeled cells was lower than the number of cells observed in the brightfield images. There appears to be a high variability in labeling efficacies of OTL38 with the PDX breast cancer cells. We also noticed a similar trend between cell culture 1 and cell culture 2 where cell culture 1 exhibited overall higher

signals than cell culture 2. Internalization may have accounted for this trend. However, one can not prove beyond a doubt that the signals measured from well 1 were attributed to cells. From the previous experiment, involving PDX cells imaged in a capillary tube, we concluded theoretical results for the confocal and Nikon systems, using the Thorlabs DCC 3240N camera and a 10X objective. We predicted that the confocal system would attain a higher SNR by a factor of 2.5 compared to the Nikon microscope with the ThorLabs camera. The measured factor was 2.3 in the experimental results. These experimental data are consistent with the theoretical findings. The experimental results comparing the Nikon/PIXIS to the confocal yielded a SNR ratio of 15, as opposed to the predicted parameter of 7.8. There is variation when comparing other data points between the confocal and Nikon/PIXIS that are consistent with the theoretical findings. The SNR ratio between the Nikon/PIXIS and Nikon/Thor was measured to be 34, as opposed to 19 in the predicted results. Unfortunately, there is only one data parameter from the Nikon/Thor for comparison in these results, so more data parameters acquired from the Nikon/Thor may yield a result more consistent with the predicted results in the previous section.

Chapter 5: Conclusion and Discussion

This thesis investigated the feasibility of employing a real-time fluorescence optical imaging system for the application of in vivo flow cytometry for detecting rare (CTCs) in vasculature. Three different optical imaging system configurations were employed: a Nikon Eclipse E600 fluorescence microscope with a PIXIS 2048B CCD camera, a Nikon Eclipse E600 fluorescence microscope with a ThorLabs DCC 3240N CMOS camera, and a Confocal Microendoscope with a ThorLabs DCC 3240N CMOS camera. We utilized fluorescent microspheres in the green spectral range 505-515 nm to determine the required SNR in fluorescence images to allow detection of CTCs. Using fluorescence microspheres we established that we could successfully detect cells in our images with an SNR of approximately 2.3 or greater using the ThorLabs DCC 3240N camera on the Nikon system. We were able to demonstrate the capability of detecting fluorescent signals in the NIR spectral band from cells fluorescently labeled with the fluorescent contrast agent OTL38, which targets the folate receptor. PDX, OVCAR3, and MCF10A cells were imaged after attempting to label them with OTL38 contrast agent. Our results show SNR levels were sufficient for real-time imaging of some PDX cells, although the fluorescence labeling of PDX cells with OTL38 was variable. OVCAR3 cells and MCF10A cells had much weaker signal levels and SNRs than what was achieved with the PDX cells. MCF10A cells were essentially used as a negative control due to their low expression of folate-receptor sites.

An important aspect of future work is to more precisely explore and quantify how effectively different cancer cells can be selectively labeled with receptor targeted contrast agents. One way to do this is to implement an in vitro flow cytometric setup in which blood

samples, containing cancer cells, are mixed with a dye that labels all cells and a receptor-targeted agent that selectively labels cancer cells. The flow cytometric measurement would allow one to quantify how accurately cancer cells can be detected from other cells in a whole blood sample. Even with control measures, it is important to realize that results can vary between cell cultures and the conditions introduced to cell cultures. It is imperative to conduct investigations as to the possible effects of trypsin on cellular receptor sites. The investigation of the possibility of internalization needs to be investigated to establish whether a fluorescent ligand is disassociating from the cell receptor site after a certain incubation time period. The possible adverse effects on cellular uptake of an infected cell line due to mycoplasma also needs to be investigated.

The next step for future work would be to fluorescently label cells in vivo. A possible method for this is to use an animal model in which fluorescently labeled cancer cells are intravenously injected into the blood stream. A window chamber can be used as a test bed to see if the labeled cancer cells can be detected through the window.

If that future work shows that the technique shows promise, long-term work involves designing, building and implementing a 2D en face imaging system that can be used for the application of in vivo flow cytometry. The systems that were evaluated in the experiments presented are not optimized for the purpose of in vivo flow cytometry. The data comparing the transmission and SNR of the three optical system configurations serve as initial imput for this process, as they provide insight into the performance characteristics necessary in a viable system. Comparing experimental results from the last experiment involving PDX cells, the confocal system showed the ability to obtain, on average, higher SNR levels than the Nikon/ThorLabs configuration by a factor of 2.3. The SNR ratio between the Nikon/PIXIS and the confocal system

was measured to be 15, and the SNR ratio between the Nikon/PIXIS and the Nikon/ThorLabs was measured at 34. However, it is important to realize that the FOV for the Nikon/ThorLabs setup was smaller than the confocal system and the spatial resolution was higher. Investigating what system FOV and resolution are necessary to effectively locate a region of interest and adequately resolve fluorescent cells is another important aspect of future work. Looking into optimizing optical and digital performance parameters such as transmission, the NA in image space, the system PSF, and camera system are critical for devising a reliable imaging system for in vivo flow cytometry. Answering the question of whether a confocal imaging system with optical sectioning capabilities is necessary to localize detected signal at a specific depth within a vessel is another aspect of developing an in vivo flow cytometry system. This research began to investigate the idea of in vivo flow cytometry, but much remains to be done to realize a practical and clinically useful instrument.

Bibliography

[1] Y. Li, Z. Fan, G. Liu, X. Tan, C. Wang, and Z. Gu, “Circulation times of hepatocellular carcinoma cells by in vivo flow cytometry,” vol. 8, no. 10, pp. 953–956, 2010.

[2] Flow Cytometry A Basic Introduction. Retreived from flowbook.demovosoftware.com/chapter-1-introduction-0

[3] Precision Engineering to Target Disease. Retrieved from www.ontargetlaboratories.com/technology.html

[4] Y. Ding, J. Wang, Z. Fan, D. Wei, R. Shi, Q. Luo, D. Zhu, and X. Wei, “Signal and depth enhancement for in vivo flow cytometer measurement of ear skin by optical clearing agents,” *Biomed. Opt. Express*, vol. 4, no. 11, pp. 2518–26, 2013.

[5] W. He, H. Wang, L. C. Hartmann, J. X. Cheng, and P. S. Low, “In vivo quantitation of rare circulating tumor cells by multiphoton intravital flow cytometry,” *Proc. Natl. Acad. Sci. U. S. A.*, vol. 104, no. 28, pp. 11760–11765, 2007.

[6] E. I. Galanzha and V. P. Zharov, “Circulating Tumor Cell Detection and Capture by Photoacoustic Flow Cytometry in Vivo and ex Vivo.,” *Cancers (Basel).*, vol. 5, no. 4, pp. 1691–738, 2013.

[7] L. Golan, D. Yeheskely-Hayon, L. Minai, E. J. Dann, and D. Yelin, “Noninvasive imaging of flowing blood cells using label-free spectrally encoded flow cytometry,” *Biomed. Opt. Express*, vol. 3, no. 6, p. 1455, 2012.

[8] A. Rouse, “MULTI-SPECTRAL CONFOCAL MICROENDOSCOPE FOR IN-VIVO IMAGING,” pp. 20-26, 2004.

[9] T. Wilson, *Confocal Microscopy*: 1990. pp. 22-24

[10] T. Wilson and C. Sheppard, *Theory and Practice of Scanning Optical Microscopy*:Second Edition. 1985. pp. 12-20

[11] J.W. Goodman, *Introduction to Fourier Optics:* Third Edition. 2005. pp. 63-78

[12] PIXIS 2048. Retrieved from http://www.princetoninstruments.com/userfiles/files/assetLibrary/Datasheets/Princeton_Instruments_PIXIS_2048_eXcelon-N5_1-10_22_14.pdf

[13] T. Wu, “DESIGN OF CONFOCAL MICROENDSCOPY FOR FALLOPIAN TUBE IMAGING AND In the Graduate College,” pp. 1–171, 2015.

[14] ThorLabs DCC3240N. Retrieved from https://www.thorlabs.com/newgrouppage9.cfm?objectgroup_id=4024&pn=DCC3240N

[15] E2V Data Sheet. Retrieved from http://www.e2v.com/content/uploads/2014/02/DSC_EV76C661.pdf

[16] Fluorescence Filter Combinations. Retrieved from http://www.microscopyu.com/techniques/fluorescence/nikon-fluorescence-filter-sets.

[17] Princeton Instruments Catalog of High Performance Digital CCD Cameras. Retrieved from ftp://ftp.princetoninstruments.com/Public/Manuals/Old%20Catalogs/imagcat(d).pdf

[18] G. D. Guglielmo, P. Drake, P. Baass, "Insulin receptor internalization andsignalling," Molecular and Cellular Biochemistry., vol. 182, no. 1-2, pp. 59-63, 1998.

[19] S. C. Parija, *Textbook of Microbiology and Immunology*: Second Edition. pp.404